Nanoscale

REVIEW

Check for updates

Multicolored inorganic electrochromic materials: status, challenge, and prospects

Chengyu Jiang,[a,b] Rui Ge,[a,b] Chenchen Bian,[c] Lirong Chen,[a,b] Xingru Wang,[a,b] Yang Zheng,[a,b] Gang Xu,[b] Guofa Cai [ID] *[c] and Xiudi Xiao*[d,e]

Against the backdrop of advocacy for green and low-carbon development, electrochromism has attracted academic and industrial attention as an intelligent and energy-saving applied technology due to its optical switching behavior and its special principles of operation. Inorganic electrochromic materials, represented by transition metal oxides, are considered candidates for the next generation of large-scale electrochromic applied technologies due to their excellent stability. However, the limited color diversity and low color purity of these materials greatly restrict their development. Starting from the multicolor properties of inorganic electrochromic materials, this review systematically elaborates on recent progress in the aspects of the intrinsic multicolor of electrochromic materials, and structural multicolor based on the interaction between light and microstructure. Finally, the challenges and opportunities of inorganic electrochromic technology in the field of multicolor are discussed.

1. Introduction

The magnificent colors in nature provide people with a sense of security for survival and greatly enrich human cognition of beauty. Color is an essential element in our lives, as it is an intuitive way for us to perceive the world. But monotonous color tones may cause visual fatigue, and low color purity can decrease the quality of viewing. From black and white TVs to color TVs, from liquid crystal displays (LCDs) to light emitting diodes (LEDs) with clearer pictures and more vivid colors, people are pursuing better visual effects.[1] Therefore, developing multicolored display materials and devices not only meets the demand for a high-quality life but will also be an important research direction in the future. Electrochromic (EC) materials are a kind of smart material that can reversibly and persistently change color, transmittance, or other optical pro-

perties through electrochemical redox reactions under external electrical stimulation.[2–4] With the characteristics of optical modulation, they offer great potential for various color-adjustable applications, promoting research and development in related fields, such as electronic displays,[5,6] camouflage,[7,8] indicators of energy storage states, *etc*.[9–12] As a non-emissive type of display, it is worth noting that electrochromic displays can maintain a colored state without external voltage over a certain period of time, which is called color memory performance. Compared with commercial emissive displays, their energy savings can be >99% higher than that of e-ink readers or related LED devices when displaying continuously for 2 days, which will bring about revolutionary progress in energy-saving displays.[13]

Inorganic electrochromic materials and organic electrochromic materials are two widely studied types of electrochromic material.[14] Compared with organic electrochromic materials represented by organic small molecules,[15,16] and conductive polymers,[3,17,18] inorganic electrochromic materials are more suitable for practical applications due to their excellent chemical stability and long-term durability.[19–21] Since Deb *et al.* reported the first instance of inorganic electrochromic materials and devices when studying amorphous and crystalline tungsten oxide at Cyanamid Corporation in 1969, inorganic electrochromic materials have experienced rapid development over the past 50 years.[22,23] The coloring mechanism of inorganic electrochromic materials represented by transition metal oxides (TMOs) and Prussian blue (PB) and its analogs (PBAs) is related to the presence of unpaired electrons in the d orbital. Under certain conditions, a reversible transformation

[a]School of Energy Science and Engineering, University of Science and Technology of China, Hefei 230026, China
[b]Guangdong Provincial Key Laboratory of New and Renewable Energy Research and Development, Guangzhou Institute of Energy Conversion, Chinese Academy of Sciences, Guangzhou 510640, China
[c]Key Laboratory for Special Functional Materials of Ministry of Education, National & Local Joint Engineering Research Center for High-efficiency Display and Lighting Technology, School of Materials and Engineering, and Collaborative Innovation Center of Nano Functional Materials and Applications, Henan University, Kaifeng 475004, China. E-mail: caiguofa@henu.edu.cn
[d]School of Physics and Optoelectronics, South China University of Technology, Guangzhou 510640, China
[e]State Key Laboratory of Luminescent Materials and Devices, South China University of Technology, Guangzhou 510640, China. E-mail: xiaoxiudi@scut.edu.cn

occurs to form a mixed-valence state, where the color varies with the valence state and concentration of ions.[24] Limited types of ions in different valence states restrict the color gamut of inorganic electrochromic materials. These daunting obstacles still need to be overcome in multicolored tuning. Therefore, improving the monochromatic properties and universality of color adjustment of inorganic electrochromic materials has become a hotspot in the field of electrochromic materials.[25]

Currently, there are three main strategies to achieve multicolor based on inorganic electrochromic materials: intrinsic color,[26–28] structural color,[29,30] and stacked color (Fig. 1).[31,32] Vanadium ions in vanadium oxide can alter the proportions of distinct valence states with voltage, presenting yellow, green, and blue, respectively.[33] Other transition metals can be expected to replace the coordinating iron in the PB skeleton to obtain additional color presentation.[34] Inspired by combining three primary colors to form other colors, color characteristics of different materials can also be combined to achieve color superposition. Therefore, designing a reasonable superposition strategy has been considered an important way to achieve multicolor. Moreover, photonic metamaterials with special optical properties can adjust light interference, diffraction, and reflection, such as WO_3 stacking structures forming distributed Bragg reflectors,[35] inverse opal structures,[36–38] and photonic crystals.[39,40] This kind of material has the ability to interact with light and enhance/attenuate the specific wavelength of light. At the same time, to artificially regulate the desired reflected color, the introduction of the Fabry–Pérot (F–P) cavity is expected to realize panchromatic coverage and high color saturation.[41–43] At the microscale, nanoparticles and plasmonic materials can be electrochemically charged in a capacitive manner, and light is coupled to plasmonic materials by the resonance excitation of freely charged carriers as surface plasmon resonance (SPR), which could be achieved by regulating nanocrystal size, changing the host environment, or doping/injecting charges to realize a wide range of spectral

tunability.[44,45] Recently, multicolor based on noble metal nanoparticles has been created through reversible electrochemical deposition. In addition, the stacked structure of electrochromic devices provides a good foundation for color superposition and endows each layer with different colors. Extensive studies have shown that the above-mentioned methods are crucial for enhancing the color tone and purity of inorganic electrochromic materials in multicolored tuning.[46,47]

Although there have been many reviews focusing on organic electrochromic materials for multiple colors, the topic of inorganic electrochromic materials for achieving multicolor is rather rare. This review systematically elaborates on both intrinsic color changes resulting from material itself and structure-related multicolor. Finally, based on the current research status of inorganic electrochromic materials, a proposal is made for the development trend in multicolor.

2. Strategies of multicolor

On the one hand, inorganic electrochromic materials exhibit various colors related to different valence states and the concentration of internal transition metal ions, which is referred to as the intrinsic color of materials. On the other hand, colors generated by the interaction between the microscopic structure and light are called structural colors. To accurately grasp the electrochromic performance of materials and devices, researchers have introduced important parameters, such as optical modulation, switching time, and cycling stability, to evaluate their performance.[48,49] Optical modulation (ΔT) refers to the difference in transmittance or reflectance before and after coloration at a certain wavelength. The switching time between different colors should be as short as possible, reflecting rapid color conversion. Excellent cycling stability is manifested by maintaining stable optical modulation and structure after long-term operation. Since multicolored appli-

Chengyu Jiang is currently pursuing his Master's degree under the supervision of Prof. Xiudi Xiao at the University of Science and Technology of China. His current research interests focus on inorganic electrochromic materials.

Chengyu Jiang

Guofa Cai is a full professor in the School of Materials and Engineering at Henan University and Outstanding Youth Foundation Scholar of the National Natural Science Foundation. He obtained his PhD in Materials Science and Engineering at Zhejiang University in 2014. Then he went to Nanyang Technological University in Singapore as a Research Fellow. His research interests focus on the design and

Guofa Cai

fabrication of electrochromic films, flexible transparent conductive electrodes, as well as solid-state transparent electrolytes with high stability.
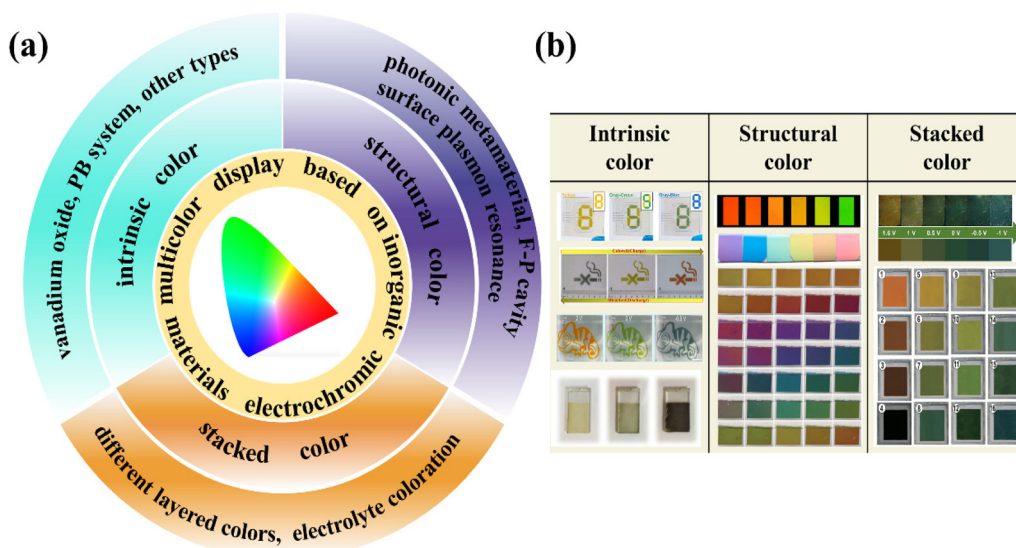
(a)

(b)

Fig. 1 (a) Schematic diagram of multicolor based on inorganic electrochromic materials. (b) Specific pictures of different color types.

cation based on inorganic electrochromic materials relies on the ability to switch between different colors, quantification of color is an important aspect to evaluate the performance of multicolored electrochromic materials. Colorimetric analysis is usually based on the scheme formulated by the Commission Internationale de ĺEclairage (CIE), in which CIE XYZ and CIE LAB are the two commonly used systems of color coordinates. All colors in the CIE XYZ color space are quantified by a three-attribute system: the red–blue ratio, the green–blue ratio, and the relative brightness; the CIE LAB color model is composed of the brightness (L^*) and color-related a^* and b^*, where a^* represents the range from magenta to green, and b^* represents the range from yellow to blue. The contrast in color (ΔE) between two different states can be expressed by the following formula (1):

$$\Delta E = \sqrt{[(L_2^* - L_1^*)^2 + (a_2^* - a_1^*)^2 + (b_2^* - b_1^*)^2]} \tag{1}$$

Xiudi Xiao is a full professor in the School of Physics and Optoelectronics at South China University of Technology. She obtained her PhD in Shanghai Institute of Optics and Fine Mechanics, Chinese Academy of Sciences in 2010. Her research interests include stimuli-responsive photo-electronic functional systems, and color changing devices based on thermochromic material or electrochromic materials.

Xiudi Xiao

2.1 Intrinsic multicolor modulation

Optical properties of transition metal oxides can be modulated within visible and infrared ranges by adjusting the external voltage, which is a result of the effective insertion/extraction of electrons from the electrode and ions from the electrolyte during the electrochromic process.[50,51] Among inorganic electrochromic materials, transition metal oxides are thought to be one of the most promising types. Specific oxide distributions are illustrated in Fig. 2, where WO_3,[52,53] Nb_2O_5,[54,55] TiO_2,[56,57] MoO_3,[58,59] and Ta_2O_5 have the ability to realize cathodic coloring with external voltage.[60] The EC performance of WO_3 has been extensively studied. It was found that it can display a deep blue color with the insertion of lithium ions while it becomes transparent upon extraction of Li ions. Correspondingly, electrochromic phenomena have also been observed in certain anodic coloring materials, such as MnO_2, Cr_2O_3, NiO, IrO_2, and Co_3O_4.[61–68] It is worth noting that V_2O_5 is the only oxide that shows multicolored transformation toward both cathodic and anodic reactions. In addition, these metal oxides all share similar octahedral crystal structures and electronic band structures with intrinsic empty d orbits.[69] They can usually be readily filled upon charging, leading to vivid coloration due to inter-band transition.[70] However, the diversity of colors is somewhat limited, whether used in cathodic or in anodic materials.

2.1.1 The multicolor of vanadium oxide films. Different from other transition metal oxides, vanadium ions in vanadium oxides exist in multiple valence states including V^{2+}, V^{3+}, V^{4+}, and V^{5+}, which are responsible for distinct colors. In particular, pentavalent (V^{5+}), tetravalent (V^{4+}), and trivalent (V^{3+}) correspond to yellow, blue, and green, respectively, giving it the beautiful nickname "Vanadis" after the Norwegian goddess of beauty. Among TMOs, V_2O_5 is applied as a promising inorganic material due to its multicolor behaviors which
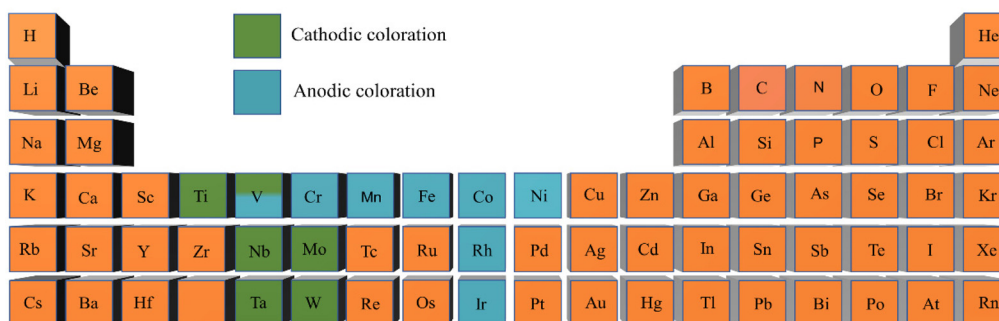
Fig. 2 Periodic table representing electrochromic elements with anodic and cathodic coloration behavior.

can exhibit more than two colors, typically yellow, green, and blue, upon voltage modulation. The color-changing mechanism of V_2O_5 can be represented by eqn (2), where M^{n+} refers to positively charged M ions of n-valence, including Li^+, Zn^{2+}, and Al^{3+}.

$$V_2O_5 + xM^{n+} + xne^- = M_xV_2O_5 \qquad (2)$$
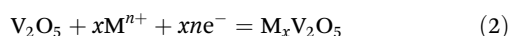
However, the low conductivity, significant volume expansion during cycling of bulk V_2O_5,[71,72] and long response time limit its widespread application. Constructing different nanostructures is expected to greatly shorten the ion diffusion path,

thus reducing coloration time while increasing color contrast. The construction of a one-dimensional structure of V_2O_5 is considered an effective method to overcome existing problems. Yang *et al.* successfully prepared one-dimensional V_2O_5 nanobelts using industrial V_2O_5 powder as a precursor (Fig. 3a),[73] and these nanobelts exhibited significant electrochromic properties and reversible multicolored changes from gray to yellow to brick-red, which resulted from the different valence state changes of vanadium ions during electrochromic processes. Even at a high current density, reversible and rapid color changes could effectively monitor energy storage levels, demonstrating the potential for its widespread use in energy
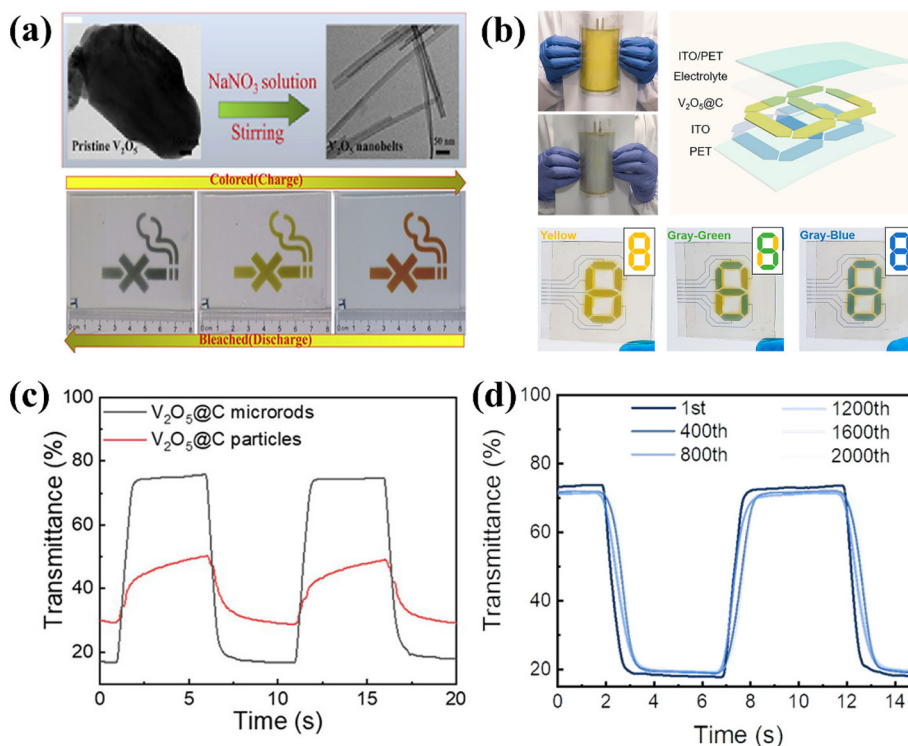

Fig. 3 Summary of the one-dimensional structures of vanadium oxide. (a) The fabrication and optical performance of V_2O_5 nanobelts. Adapted with permission from ref. 73. Copyright 2020, Elsevier. (b) Digital photographs of a large-scale EC device (10 cm × 10 cm) under applied voltages of 2.5 V (top) and −2.5 V (bottom) and digital photographs and diagrams of digital numbers "8" (yellow), "5" (gray-green), and "8" (gray-blue). (c) *In situ* transmittance responses for EC electrodes. (d) Cycling stability of V_2O_5@C microrods. (b–d) Adapted with permission from ref. 74. Copyright 2022, American Chemical Society.

storage devices. Limited by the poor electron conductivity and slow ionic diffusion in V_2O_5, an alternative solution to tackle the problems was presented through the synthesis of V_2O_5@C one-dimensional microrod EC electrodes.[74] A large (10 cm × 10 cm) EC device consisting of V_2O_5@C microrod EC electrodes was assembled with polymer gels as electrolytes, which exhibited multicolor changes even in the bent state. Through independently applying voltage to different areas, colorful patterns of a digital display device prepared by spray-coating the microrod ink across a mask were observed, including yellow "8", gray-green "5" and gray-blue "8" (Fig. 3b). In addition, the synergistic effect between V_2O_5 and C leads to ultrafast coloration and bleaching time ($\tau_c \sim 1$ s, $\tau_b \sim 1$ s) and a stable cyclic life (Fig. 3c and d). Based on the spray coating method, there is potential to manufacture flexible large-sized multicolored display devices.

Compared with a one-dimensional nanostructure, a multidimensional structure has a larger surface area and provides more active sites for the reaction, which greatly improves the speed of the color conversion. However, complex structures with enhanced electrochemical properties can obscure the originally desired colors by the optical scattering effect.[75,76] Two-dimensional (2D) materials with high packing density can decrease the scattering sites such as surface roughness and internal voids, which is beneficial for accurate color modu-

lation over a wider range. As shown in Fig. 4a, Ki-Seok An *et al.* prepared 2D V_2O_5 nanosheets by oxidizing single-layer V_2CT_x MXene.[77] Owing to the high aspect ratio, the nanosheets showed clear color transitions from yellow to green to blue, as depicted in Fig. 4b. The excellent multicolored transformation ability of the two-dimensional V_2O_5 nanosheets was demonstrated by the large triangular region in the CIE-1931 chart (Fig. 4c). Similarly, Li *et al.* synthesized coral-shaped V_2O_5 on an indium-doped tin oxide (ITO) substrate through annealing processes,[78] exhibiting multicolored characteristics (yellow, blue-green, and olive) which were associated with the status of the vanadium ion. In order to verify the above idea, the valence states of vanadium ions based on the V $2p_{3/2}$ core peak spectra are recorded in Table 1. As the voltage was lowered from +1 V to −1 V, the ratio of V^{5+}/V^{4+} decreased continuously, while the V^{3+} content gradually increased, corresponding to the color transformation from orange to blue and finally to olive (Fig. 4d). In terms of practicality, electrochromic films with high stability and large color contrast show military prospects in advanced adaptive camouflage. The SnO_2/V_2O_5 core/shell structure exhibited good cycling stability,[79] and a reversible color change between yellow, green, and blue can be observed. The corresponding color changes suggested that it would be hidden in natural conditions such as deserts, oases, and oceans (Fig. 4e).
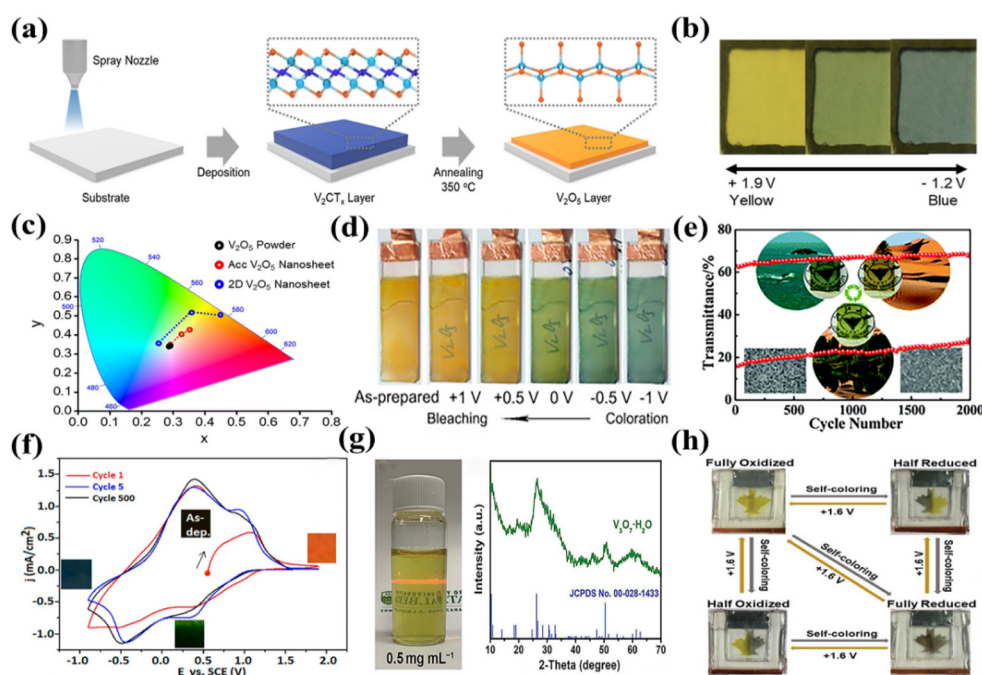

Fig. 4 (a) Schematic for the fabrication of an ECD based on a V_2CT_x-derived 2D V_2O_5 nanosheet. (b) Digital image of EC. (c) Color coordinates of V_2O_5 powder, Acc, and 2D V_2O_5 nanosheet-based ECDs mapped on a CIE-1931 chromaticity diagram. (a−c) Adapted with permission from ref. 77. Copyright 2022, Elsevier. (d) Digital photographs of the coralline V_2O_5 architecture under different voltages compared with the as-prepared film. Adapted with permission from ref. 78. Copyright 2016, Elsevier. (e) Cyclic test of light transmittance of SnO_2@V_2O_5 core−shell structures and multi-color properties adapted to deserts, oases, and oceans. Adapted with permission from ref. 79. Copyright 2019, Royal Society of Chemistry. (f) Cyclic voltammograms of V_2O_3 films. Adapted with permission from ref. 80. Copyright 2018, American Chemical Society. (g) Photograph of the V_3O_7 colloid and the XRD pattern of the nanoparticles. (h) The functionalities of the electrochromic battery display. (g and h) Adapted with permission from ref. 81. Copyright 2020, Wiley-VCH.

Table 1 Fitting results of V2p$_{3/2}$ core XPS spectra of the coralline V_2O_5 nanorod architecture under different polarized potentials. Adapted with permission from ref. 78. Copyright 2016, Elsevier

Different polarized potentials	Binding energy for V^{5+}	V^{5+} peak area percent	Binding energy for V^{4+}	V^{4+} peak area percent	Binding energy for V^{3+}	V^{3+} peak area percent
+1 V	517.1 eV	88.4%	515.4 eV	11.6%		
+0.5 V	517.1 eV	81.5%	515.8 eV	18.5%		
0 V	516.9 eV	65.2%	515.5 eV	34.8%		
−0.5 V	516.9 eV	80.2%	515.7 eV	8.8%	515.1 eV	11%
−1 V	516.8 eV	67.4%	515.7 eV	12.1%	515.0 eV	20.5%

In addition to the commonly studied V_2O_5, vanadium oxides also include V_2O_3 and V_3O_7. For instance, Aline Rougier *et al.* successfully prepared V_2O_3 powders from a polyol-mediated synthesis that was easily controlled in large-scale production,[80] and the unknown EC characteristics of V_2O_3 were revealed for the first time. A similar color change of green–blue–orange was observed between V_2O_3 and V_2O_5 (Fig. 4f). For the reduced state of light blue, the L^*, a^*, and b^* values were 26, −15, and −6, respectively, while for the bright orange oxidation state, the L^*, a^*, and b^* parameters were 68, 11, and 56, respectively. The contrast in color (ΔE) between the two states was 79. Furthermore, it was found that V_2O_3 held exceptional memory effects. The colored V_2O_3 film was exposed to air at room temperature for 30 days without voltage. The chromatic parameters did not change (Table 2), indicating its excellent color memory performance, which is attributed to the good porosity and inherent stability inside the film. Li *et al.* proposed a simple synthesis strategy of V_3O_7 colloidal nanoparticles (Fig. 4g).[81] The gray-blue to yellow color conversion of the V_3O_7 cathode was presented by the deintercalation process of Zn^{2+}, and a Zn-V_3O_7 electrochromic device was assembled at the same time. The prototype device can be reversibly switched between multiple colors, including all-yellow, all-gray-blue, and half-yellow–half-gray-blue (Fig. 4h). Both V_2O_3 and V_3O_7 prove the highly similar multicolored characteristics of V_2O_5, thus further exploration of more types of vanadium-based compounds will be a promising path in future.

2.1.2 The multicolor of PB and PBA. PB is a kind of compound containing two different states of iron ions (Fe^{2+}, Fe^{3+}), in which Fe^{2+} is linked to the C atom of CN^- through coordination bonds, and Fe^{3+} is linked to the N atom of CN^- through coordination bonds to form a three-dimensional framework structure.[82] In 1978, Diesbach first discovered its electrochromic properties. Subsequently, PB was used to synthesize new

materials with various optical properties by redox reactions. In different redox voltages, PB usually transforms between PB, Prussian white (PW), Prussian green (PG), and Prussian brown (PX). Chu *et al.* prepared PB films using the hydrothermal method to investigate its electrochromic performance, finding that the color change between colorless and blue undergoes an insertion and extraction of K^+ ions during the electrochemical process.[83] On the other hand, PG is obtained by oxidizing PB, and PX can be obtained by further oxidation of PG. The synthesis of PX is an irreversible process, and when in the bulk form, it appears brown which is different from the yellow in film form. In another study reported by Li *et al.*, PG films were prepared by a one-step hydrothermal method with a crystal structure equivalent to PB.[84] The color was related to the ratio of Fe^{3+}/Fe^{2+}, demonstrating the ability for reversible changes between green, blue, and colorless states (Fig. 5a). The open three-dimensional structure enabled PG to change color quickly, as shown by the short switching time of 1.1 seconds from green to blue and 2.4 seconds to colorless. However, despite showing rapid color transitions, there is still the problem of the limited color change range. Substituting the coordinating iron in the PB lattice is regarded as an efficient strategy to produce different PBAs with additional colors. For example, for molybdate hexacyanoferrate (MoOHCF) prepared by Liao *et al.*,[85] the brownish-red PBA exhibited a similar electrochromic color change mechanism to PB. Alkali metal ions were inserted into the lattice structure of the PBA at different voltages to bring about vivid color changes. It appeared brownish-red in the reduced state (0.51 V) and pale yellow in the oxidized state (1.17 V) (Fig. 5b). It also followed that a nickel-based PBA showed unique color changes from transparent to yellow. In the same way, a cobalt-based PBA ($K_2Co[Fe(CN)_6]$) exhibited colors from light green to reddish-brown, while the copper-based PBA ($K_2Cu[Fe(CN)_6]$) displayed colors from pale yellow to red (Fig. 5c–e).[86–89] Additionally, by controlling the ratio of different metal ions, PBAs will be endowed with special optical properties and are expected to provide opportunities for multicolored ECDs.

2.1.3 The multicolor of other composite films. WO_3 is one of the most widely studied inorganic electrochromic materials for cathodic discoloration. The transition of electrons between adjacent W atoms results in a color change of the films and high color contrast. The color-changing mechanism of WO_3 can be expressed by formula (3), where x is the number of embedded ions and A^+ is the cation (Li^+, H^+).

Table 2 The $L^*a^*b^*$ values in the blue-reduced state and orange-oxidized state of the V_2O_3 initial state and after 30 days. Adapted with permission from ref. 80. Copyright 2018, American Chemical Society

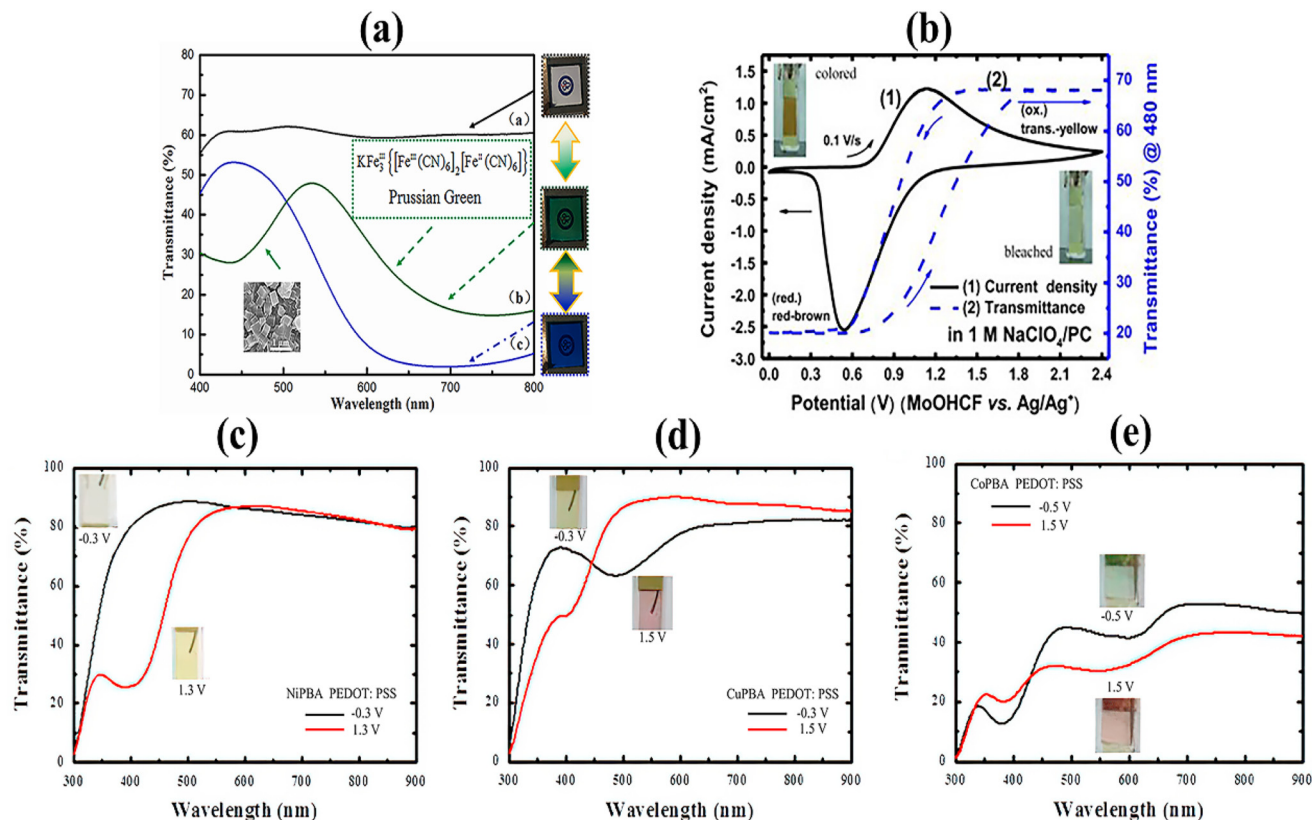| Different states	Initial			After 30 days		
	L^*	a^*	b^*	L^*	a^*	b^*
−0.9 V	26	−15	−6	28	−9	−5
+1.9 V	68	11	56	66	16	53

Fig. 5 Summary of various substituted PB complexes. (a) Transmission of light in three different states. Adapted with permission from ref. 84. Copyright 2019, Elsevier. (b) A typical cyclic voltammogram and real-time transmittance response of the MoOHCF film. Adapted with permission from ref. 85. Copyright 2016, Elsevier. (c–e) The *in situ* transmittance spectra at different potentials and the corresponding pictures: (c) Ni-PBA, (d) Cu-PBA, and (e) Co-PBA. Adapted with permission from ref. 87. Copyright 2016, Elsevier.

$$WO_3 + x(A^+ + e^-) = A_x W^{6+}_{1-x} W^{5+}_x O_3 \tag{3}$$
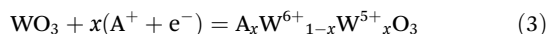
The conversion between colorless and blue states is mainly limited by W^{5+} and W^{6+}. Nevertheless, a wider color gamut can be achieved by pairing the above V_2O_5 with WO_3 through color superposition. Wu *et al.* used the solvothermal method in combination with electrodeposition to create V_2O_5 dot-decorated WO_3 nanorod arrays.[90] The average diameter of V_2O_5 dots was 2.7 nm, and the V_2O_5 dots were uniformly decorated on the surface of the nanorods. The color of the hybrid films converted from black (−1.0 V) to greenish-yellow (0.6 V) and orange-yellow (1.5 V), in which the black color was a combination of blue (colored WO_3) and orange (colored V_2O_5), respectively (Fig. 6a). In addition to this hybrid array structure, controlling the number of layers of co-assembled V_2O_5 and $W_{18}O_{49}$ nanowires and the ratio of the two nanowires,[91] make it easy to control the transmittance and color of the film. In the work reported by Yu *et al.*, dynamic multicolor changes of the film based on the Langmuir–Blodgett technique were realized. As shown in Fig. 6b, when 2, 0, and −0.5 V voltages were applied, the film appeared light orange, green, and gray, respectively. The light orange and green variations of the film can be attributed to the electrochromic properties of V_2O_5 nanowires, while the gray was a combination of the green of

V_2O_5 and the blue of $W_{18}O_{49}$ nanowires at −0.5 V bias. Under a certain mass ratio, the number of layers of nanowires was the key to influencing color saturation. By comparing the CIE color coordinates of 1, 3, 5, and 10 layers, it was found that the CIE color coordinates were closer and closer to the edge of the coordinate with an increase in the number of layers. This indicated that the color became more and more vivid, and color saturation could be customized by adjusting the number of layers of the nanowire films (Fig. 6c and d).

Apart from typical transition metal oxides, researchers have been looking for other types of inorganic electrochromic material. In 2001, Philippe first identified cadmium chalcogenide (CdS) as an inorganic electrochromic material.[92] Meanwhile, CdS quantum dots (QDs) exhibited excellent electrochromic properties. The size-dependent optoelectronic properties, associated with the electron transfer and photon transition of surface energy states, can be improved by introducing transition metal oxides. Subsequently, researchers systematically studied the multicolored properties of WO_3 film modified with CdS QDs.[93] It was found that the initial film was yellow. When Cd^{2+} was reduced to Cd^+, CdS films slowly turned from yellow to black in the process of applying a negative voltage. At −0.9 V, only some of the Cd^{2+} was reduced. At this moment, the film appeared a complex green consisting of blue (reduced
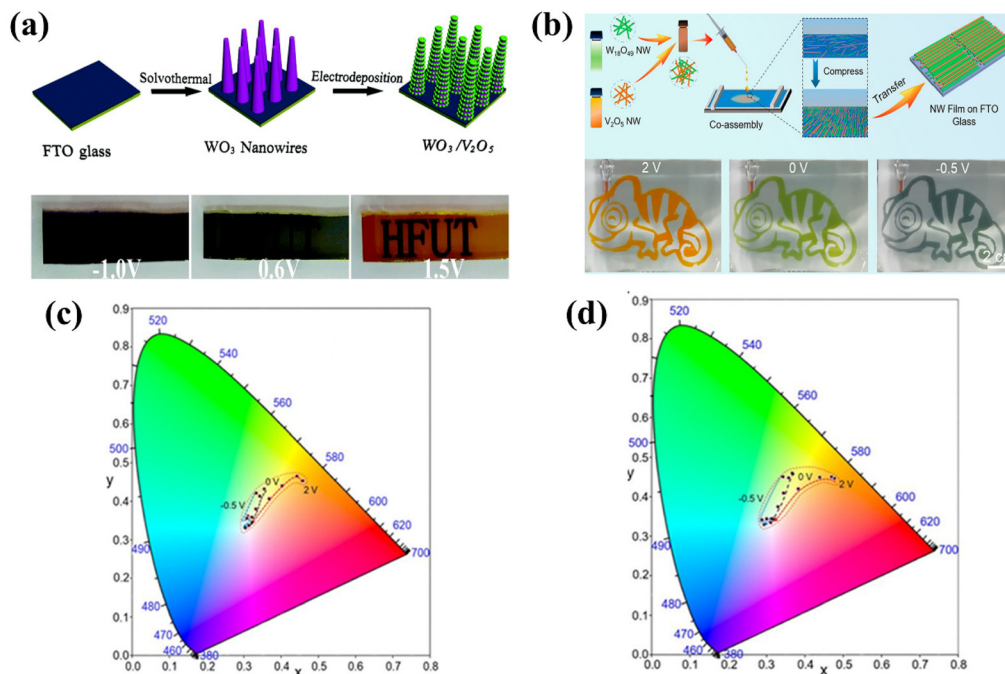
Fig. 6 Summary of common transition metal oxide recombination. (a) Schematic diagram of the formation process of WO_3/V_2O_5 hybrid films and digital photographs of the hybrid films at voltages of −1.0 V, 0.6 V and 1.5 V. Adapted with permission from ref. 90. Copyright 2018, Royal Society of Chemistry. (b) Schematic illustration for assembling $W_{18}O_{49}$ and V_2O_5 NWs on a fluorine-doped tin oxide substrate and photographs at different colored states. (c and d) CIE color coordinates of samples of 3/5 layer co-assemblies (mw : mv = 3 : 1, 3 : 3, and 3 : 5) under different applied voltages of 2 V, 0 V, and −0.5 V. (b−d) Adapted with permission from ref. 91. Copyright 2021, American Chemical Society.

WO_3), yellow (initial CdS), and black (reduced CdS). At −1.7 V, Cd^{2+} was completely reduced, and the films transformed to black (Fig. 7a). When a reverse voltage was applied, the film was composed of partially oxidized CdS and appeared brown. The complex color conversion process of the films can be analyzed through specific values in the color space coordinate diagram (Fig. 7b). This work not only exhibited a new type of composite electrochromic material but also obtained insights into inorganic electrochromic materials from metal oxides to metal chalcogenides. Through one minute of electrodeposition, double-layer hydroxide films with ultrafast transition kinetics were designed,[94] which also exhibited highly reversible yellow–green–brown multicolored performance (Fig. 7c). This composite hydroxide was based on the integrated physical and chemical properties of different electrochromic materials to produce excellent performance, providing an important reference for commercial multicolored applications (Fig. 7d). Likewise, a red–green–blue–yellow (RGBY) film was successfully obtained by electrodeposition of iron hexacyanoferrate (FeHCF) and molybdate hexacyanoferrate (MoOHCF) on ITO glass.[95] The colors of the RGBY film were red, blue, green, and yellow under applied voltages of −0.8, +0.6, +1.2, and +1.8 V, respectively (Fig. 7e). It is worth noting that this is the first reported inorganic monolayer with four typical color states. If the RGBY film is used to make electrochromic pixels, each pixel can manifest four color states. Compared to traditional three-color pixels, the RGBY film could increase resolution by

three times, which means that the storage capacity for information will be greatly upgraded by multicolor. The excellent multicolor performance of RGBY film is attributed to the open 3D framework structure, which can accommodate enough intercalated/extracted alkali metal cations. The development of pixelated electrodes and electrochromic devices based on RGBY thin films demonstrates significant potential in the field of non-emissive displays.

The advances in the intrinsic colors of materials are impressive, but they also reveal the significant restrictions of polychromatism based on intrinsic color. The issue of a limited color gamut still exists whether it is polychromatism of vanadium oxides or the combination of multiple material colors. Besides, the purity of the color is difficult to guarantee. Full-color gamut with sufficient purity has a long way to go, which is forcing people to look for more efficient ways to solve the above problems.

2.2 Polychromatism of optical structures

With the rapid development of optoelectronics, optical structures represented by optical resonators, which can produce strong optical fields and enhance light–matter interactions, have been introduced into inorganic electrochromic material for structural color generation. By assembling inorganic electrochromic materials with suitable optical resonators, all colors in the whole visible spectrum can be obtained, making it possible to address the problem of multicolored tuning.
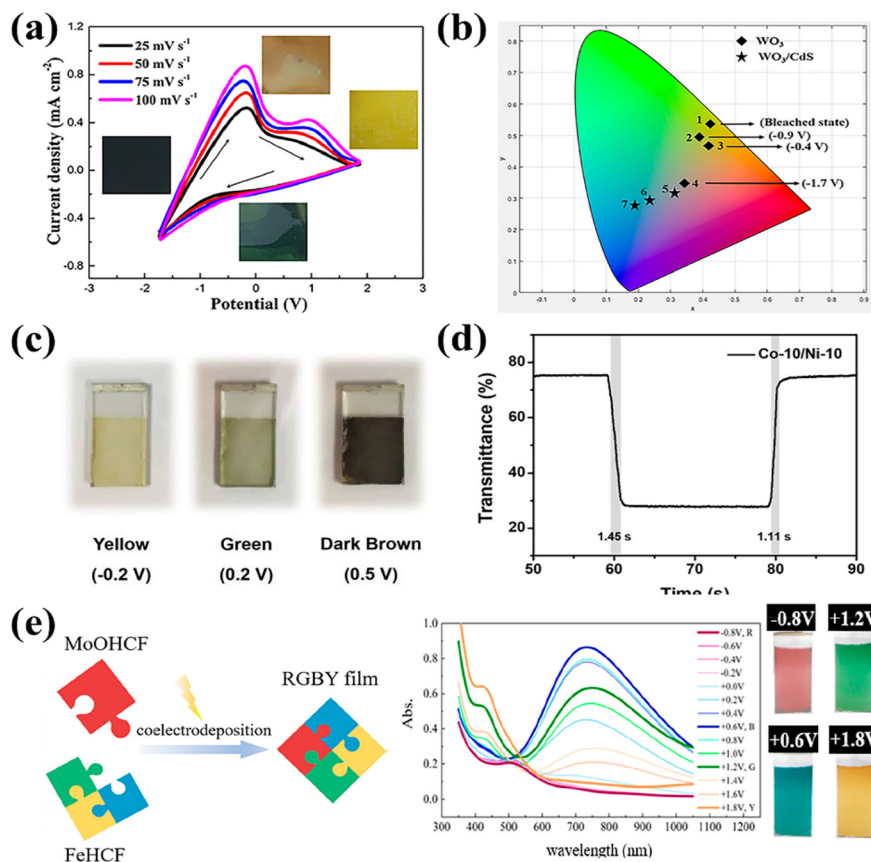
Fig. 7 (a) Cyclic voltammetry curves of CdS/WO₃ film with different scanning rates, with color photographs of CdS/WO₃ film at different potentials presented in the inset. (b) CIE diagram of WO₃ film and CdS/WO₃ film at different potentials. (a and b) Adapted with permission from ref. 93. Copyright 2023, Elsevier. (c) Digital photographic images of Co-10/Ni-20 film in various potentials. (d) The response time of Co-10/Ni-10 film. (c and d) Adapted with permission from ref. 94. Copyright 2020, Elsevier. (e) Schematic diagram of the formation process of RGBY hybrid film. Absorption spectrum (left) and digital photographs (right) of RGBY film from −0.8 V to 1.8 V. Adapted with permission from ref. 95. Copyright 2020, American Chemical Society.

Thus, exploring new platforms that provide strong optical confinement and controllable light–matter interactions embodies emerging research trends for better multicolored performance.

2.2.1 The multicolor of photonic metamaterials. Photonic metamaterials are artificially designed materials that contain nanostructures that interact with light and produce physical effects such as scattering, diffraction, and interference of incident light, which produce structural colors. Compared with the intrinsic color of materials, structural color shows obvious advantages: (1) The generation of color depends on the microstructure, so the color is hard to fade. (2) The light intensity will be enhanced by interference and diffraction. (3) The range of colors changes with the direction of the incident light and the direction of observation. (4) The color changes with the dielectric environment. The appearance of structural colors provides a range of exciting possibilities to solve the problems of intrinsic colors. In recent years, electrochromic materials combined with photonic metamaterials have gradually become the focus of research. Liu *et al.* proposed a single-step grazing angle deposition (GLAD) using electron beam evaporation to alternately deposit WO₃ layers with different porosities

(refractive indices). Based on the periodically nanostructured WO₃ films, a schematic diagram of electrochromic distributed Bragg reflectors (ECDBRs) is shown in Fig. 8a. By adjusting the deposition angle and the thickness of the WO₃ electrochromic layer, the Bragg wavelength of ECDBRs can be precisely and reversibly changed in the visible light range under a small bias voltage. The reflectance spectra of three designed 4-bilayer ECDBRs with various film thicknesses are shown in Fig. 8b, in which the central reflection wavelengths of this photonic crystal structure were located at 450, 550, and 650 nm, respectively. The ECDBRs showed clear and unique color changes under different electrical stimulation, while dense WO₃ film without periodic structures did not appear to show any obvious reflection color. This suggested that the optical properties of ECDBRs are a result of the combined effects of structural coloration and electrochromic properties (Fig. 8c). The cause of multicolor can be explained as the photonic band gap in the wavelength region being of the same order of magnitude as the periodicity. The constructive reflection of specific wavelengths can be generated by the alternation of the refractive index, which produces brilliant structural colors. Qu *et al.* pre-
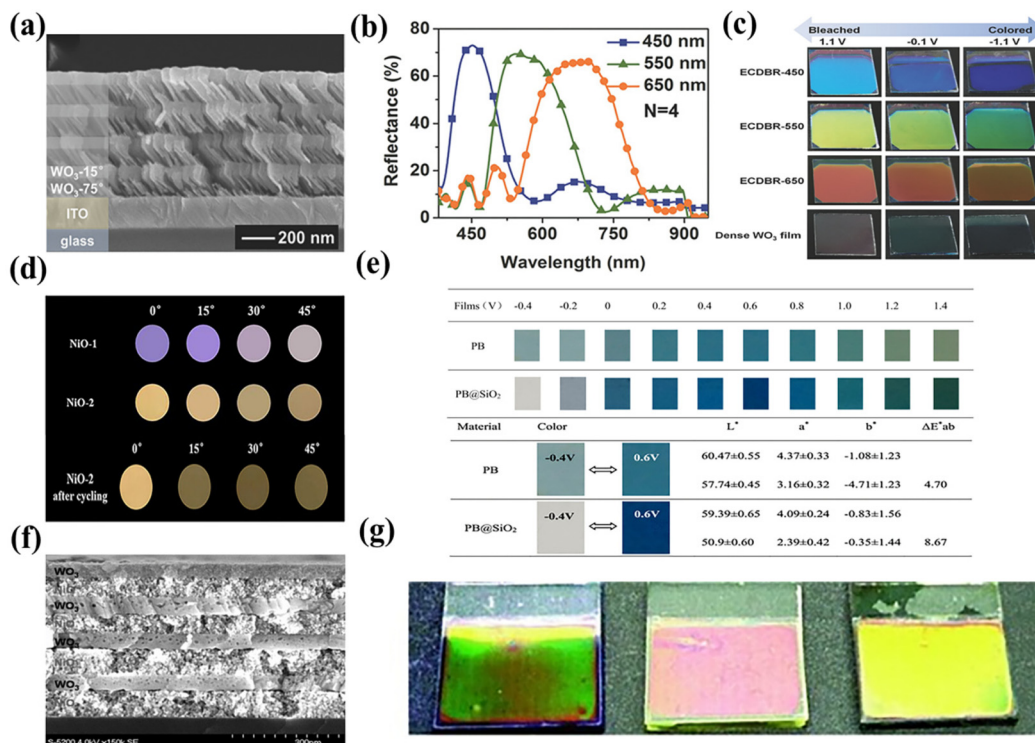
Fig. 8 (a) Cross-section and surface SEM images of a typical 4-bilayer ECDBR. (b) The reflectance spectra at normal incidence of 4-bilayer ECDBR-450, ECDBR-550, and ECDBR-650. (c) Electrochromic properties of dense WO_3 film and 4-bilayer ECDBRs with various Bragg wavelengths (λ = 450, 550, and 650 nm). (a–c) Adapted with permission from ref. 35. Copyright 2018, Wiley-VCH. (d) Digital photographs of the NiO-1 and NiO-2 samples and NiO-2 samples after cycling at different viewing angles. Adapted with permission from ref. 96. Copyright 2021, AIP Publishing. (e) Color changes and chromaticity analysis of the pure PB film and the PB@SiO_2 photonic crystal film at different voltages. Adapted with permission from ref. 97. Copyright 2021, American Chemical Society. (f) Scanning electron cross-sectional image of the NiO/WO_3 nano-porous ECBM. (g) Color effects recorded at a 60° angle for cathodic coloration. (f and g) Adapted with permission from ref. 98. Copyright 2012, Wiley-VCH.

pared multicolored NiO films with an inverse opal structure, which were unlike the typical color change between dark brown and colorless caused by the conversion of Ni^{3+} to Ni^{2+}.[96] Due to the synergistic mechanism of the intrinsic color of NiO and the structural color of the inverse opal structure, it realized a wide spectrum of blue, green, yellow, orange, and brown colors depending on pore size, wall thickness, and direction of observation (Fig. 8d). Further, the structural color which originates from the photonic band gap of photonic crystals is proved to exhibit unique optical properties including high saturation and high brightness. The enhanced electrochromic performance of composite film prepared from a PB@SiO_2 photonic crystal was observed in that the faded state was whiter,[97] and the colored state was more obviously blue, leading to greater color contrast (Fig. 8e). In contrast to single-material electrochromic photonic crystals of (Fig. 8f), an electrochromic Bragg mirror (ECBM) consisting of WO_3 and NiO multilayers did not lead to a strong spectral shift of the photonic stop-band but to a wide modulation of reflectance.[98] When a negative bias was applied, the WO_3 transformed to the colored state (decreasing refractive index) while the NiO was bleached (increasing refractive index). The increase in refractive index of one material just balances the decrease in refrac-

tive index of the other material. However, the overall effective index was slightly reduced in the case of a central wavelength of 650 nm, causing a slight blue-shift of the stop-band. Upon a positive bias, an increase in the overall effective refractive index led to a recovery of reflection. During the whole process, the alternating multilayer structure exhibited a reversible transition from green to pink to yellow (Fig. 8g). Therefore, constructing photonic metamaterials is a special method to produce new colors through the synergistic control of structural and electrochromic effects, which opens up new avenues for multicolor.

2.2.2 The multicolor of the F–P cavity. A Fabry–Pérot (F–P) cavity is an optical resonator usually made of two opposing parallel mirrors, in which the light field can be selectively enhanced by resonance to obtain two types of light: transmitted light and reflected light. When both the bottom and top mirrors are composed of thin metal films with high reflectivity, the F–P cavity formed by the multilayers would selectively transmit light of the specific wavelength rather than involving light absorption, so this multilayer structure shows transmitted light. Additionally, the reflected light is mainly generated by the asymmetric F–P cavity, which is constructed by the bottom of a metal mirror with optical thickness and the

top of a metal thin film with partial reflectivity. When the light interacts with the interface, the reflected light generated by the two interfaces of the asymmetric F–P cavity structure experiences destructive interference at the specific wavelength. An obvious reflection valley is obtained at the wavelength of the reflection spectrum, resulting in the related colors.[99,100] Obviously, regardless of any of the above structures, significant structural colors are generated by rationally utilizing the F–P cavity. Focusing on this special optical structure, the multicolor of inorganic electrochromic materials has developed rapidly. Thin WO_3 films incorporated in symmetrical stacked configurations show dynamic color change by adjustment of their dielectric constant.[101] The color purity and erasing/restoring ability were enhanced in a transmission-type device, while the color recovery ability of a dynamic color display was poor (Fig. 9a–c). It is worth noting that this design was achieved by simple film deposition without any complex nanofabrication processes, which showed surprising prospects for commercialization.

Zhao et al. carried out a lot of research into asymmetric F–P cavity structures. To gain an ability for subtle color tuning, an ultracompact asymmetric F–P cavity electrochromic device was created using partially reflective metal tungsten instead of Au as the current collector and reflector layer (Fig. 10a).[102] Strong interference was achieved by this method, which was manifested as an obvious resonance in the reflected spectrum with a maximum peak–valley fluctuation of 56% (Fig. 10b). The modulation of the spectral reflectance was regulated by the thickness of WO_3 film and the refractive indices of W film and WO_3 film. Therefore, brilliant structural color was realized due to the observed wavelength-selective reflections, as it changed with the thickness of the WO_3 layer (Fig. 10c). According to the above studies, a metal tungsten layer with a thickness of 100 nm was introduced between the ITO and WO_3 layers to construct structural multicolor.[103] There were many inter-

ference peaks and valleys in the wavelength range of 380–780 nm. In this case, the CIE 1931 color coordinates with low thickness variation were associated with the circular region from yellow to green with different tints (Fig. 10d–f). On the other hand, Fano resonance occurs when two oscillators with different damping rates are weakly coupled. Due to its sharp spectral curve, light–matter interaction is enhanced by only a small spectral shift, which significantly improves the environmental sensitivity of the resonator. Typically, the optical constant of WO_3 is strictly controlled by the degree of lithiation, which means that Fano resonance can be tuned in combination with electrochromic materials. In a structure consisting of WO_3 (60 nm)/ITO (2 nm)/Ag (18 nm)/ITO (105 nm)/Ag (130 nm), Zhao et al. found the source of the switching of reversible electrochromic conversion in the visible area from Fano to F–P resonance.[104] Upon lithiation of 24 mC (cm^2 μm)$^{-1}$, the asymmetric reflection peak (Fig. 10g) immediately appeared at about 630 nm. This indicated that F–P resonance had switched to Fano resonance even in low lithiation levels, with the structural color changing from the original light blue to purple-red in the state of Fano resonance (Fig. 10h).

Lv et al. improved the asymmetric structure again. An WO_3 electrochromic layer was used as the dielectric layer of the broadband-absorbing F–P cavity, the transition metal Cr as the broadband-absorbing layer material, and Al metal as the metal reflecting layer.[105] A wide gamut composed of red, orange, yellow, green, blue, and purple can be observed by adjusting the thickness of WO_3 (Fig. 11a). The special design offsets the defects of monotonous color and low reflectivity. Even so, the presence of a counter-electrode and electrolyte inevitably lowers the total reflectivity. This had been well addressed in the work by Andreas Dahlin et al. A unique reversed electrochromic nanostructure was presented based on WO_3, Au, and a thin Pt mirror, where the Pt reflector provided a wide color range (Fig. 11b).[106] Unlike a traditional structure, both electro-
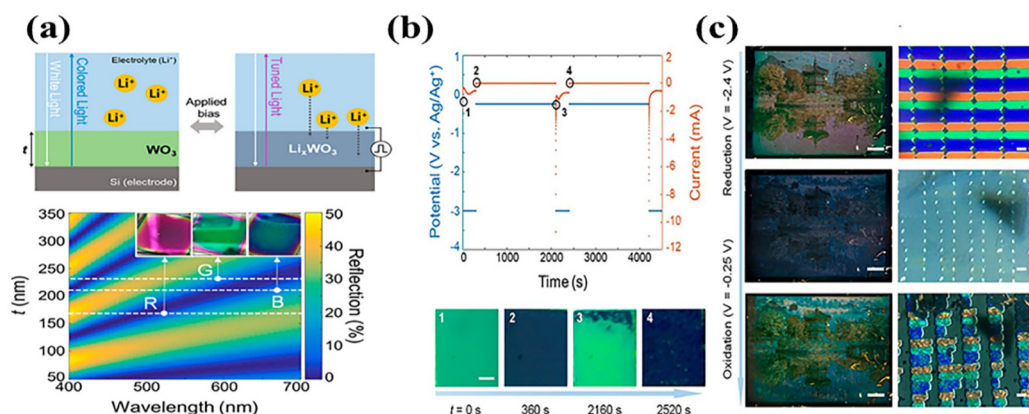

Fig. 9 (a) Schematic illustration of the transmission-type electrochromic device, t represents the thickness of WO_3 film. Target thicknesses of WO_3 for red, green, and blue pixels are determined as 100, 70, and 48 nm, respectively (inset: photographic image of fabricated color pixels). (b) Potential (blue) and current (red) during reduction and oxidation of WO_3 depending on time. Microscopic images of green color device during the repetitive color ON/OFF. Numbers 1–4 marked in the current plot correspond to the color states. (c) The left-hand photographs depict "Hyangwonjeong" in Seoul, Korea. The right-hand microscopic images correspond to each case. (a–c) Adapted with permission from ref. 101. Copyright 2020, American Chemical Society.
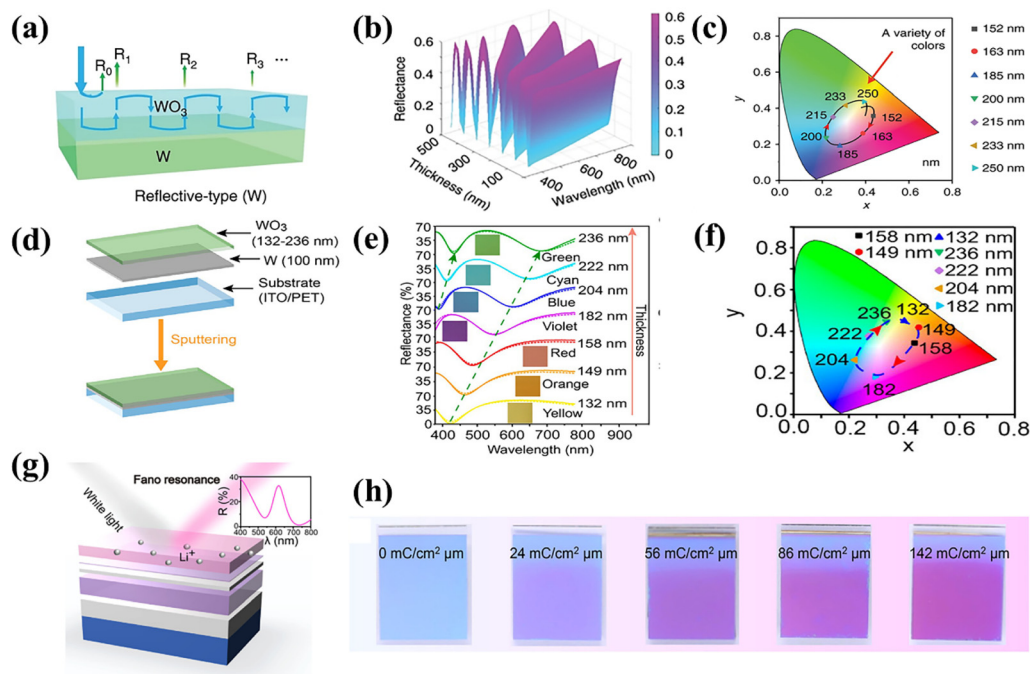
Fig. 10 (a) Schematic diagrams of light propagation. (b) Simulated transmittance/reflectance spectra. (c) Calculated color coordinates when using metallic W layers as the current collectors. (a–c) Adapted with permission from ref. 102. Copyright 2020, Springer Nature. (d) Schematic diagram of the layered structure of the F–P cavity-type electrochromic supercapacitor electrodes. (e) Simulated (dashed line) and measured (solid line) reflection spectra. Inset: optical images of the F–P cavity type electrochromic supercapacitor electrodes with different thicknesses of the WO_3 layer. (f) Color coordinates with different thicknesses of the WO_3 layer. (d–f) Adapted with permission from ref. 103. Copyright 2020, American Chemical Society. (g) Schematic diagram of the proposed photonic structure in the Fano resonance mode. Inset: reflection spectra of the proposed structure in the Fano resonance mode. (h) Optical images of the reflected color at different lithiation levels. (g and h) Adapted with permission from ref. 104. Copyright 2022, Wiley-VCH.

lyte and counter-electrodes could be placed behind the nano-structures with respect to the viewer, which demonstrated that the reversed design was no longer constrained by construction and would maintain high reflectance. However, complex processing and the use of precious metals may hinder its widespread application. A new type of porous metamaterial was reported to circumvent the critical problem of multicolor tuning. Zhao *et al.* tried putting porous nylon 66 film into an EC device containing the WO_3-W structure (Fig. 11c).[107] The synergistic effect of multiple scattering of light by distributed pores in the nylon-66 film and the interference of the F–P cavity not only achieved larger coverage of color gamut, but also solved the angle-dependent coloring of the glass/WO_3/W structure. Compared with current commercial color electronic readers and previously reported devices, this new idea was better in terms of visible angle, color gamut, wavelength modulation amplitude, and power consumption (Fig. 11d). These results indicate that cost-effective EC products of this structure will be more popular in the market.

In recent years, some researchers have gradually set their sights on looking for other media layer materials to replace WO_3. One representative example is that Zhao *et al.* gained a rich color gamut by constructing a Ti and Mn_2O_3 double-layer structure,[108] and a color change was observed from orange to yellow with thickness modulation of Mn_2O_3 (Fig. 12a). When energy storage devices were combined with the double-layer

structure, approximate colors between cyan and blue or between green and cyan can be observed during the charging/discharging process. The multicolored properties of the special structure bought new development opportunities for intelligent electrochromic energy storage devices (EESDs). In another study, a dielectric functional layer TiO_2 was introduced as the top of a symmetrical Ag-TiO_2-Ag F–P structure to prepare circular colored filters with a diameter of 25.4 mm,[109] which showed additive colors of blue, green, and red for the transmission mode and subtractive colors of yellow, magenta, and cyan for the reflection mode (Fig. 12b). In comparison to the above-mentioned oxides, cost-effective amorphous Si (α-Si) also exhibits similar electrochromic properties, which enables the thickness and refractive index of the films to simultaneously change with the degree of lithiation/delithiation. Inspired by the excellent characteristics, Bao *et al.* constructed a new FP cavity for structural color tuning by depositing an α-Si layer onto a reflective metal substrate.[110] During the Li intercalation process in Fig. 12c, the fabricated structure exhibited a consecutively controllable multicolored property. However, most F–P structures are predesigned and static, which limits the sequence of layer stacking. It is challenging to alter the features of the structure once fabricated. Interestingly, when applying the suitable voltage bias and then reversing it, Ag$^+$ ions were allowed to enter and exit through
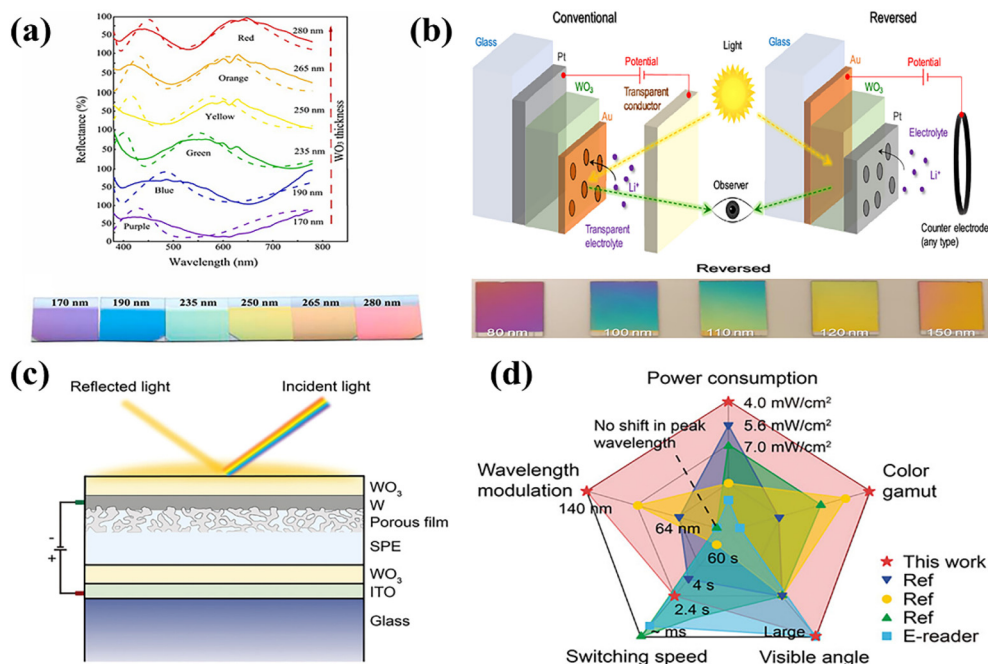
Fig. 11 (a) Measured (solid lines) and simulated (dashed lines) reflection spectra and optical images in different thicknesses of tungsten oxide. Adapted with permission from ref. 105. Copyright 2022, Elsevier. (b) Schematic illustration of reverse architectures and photographs of samples with different thicknesses of WO_3. Adapted with permission from ref. 106. Copyright 2021, American Chemical Society. (c) The structure designed by Zhao's team. (d) Performance comparison of EC displays with different references (ref) and commercial color e-readers in terms of visible angle, color gamut, wavelength modulation amplitude, power consumption, and switching speed. (c and d) Adapted with permission from ref. 107. Copyright 2023, Wiley-VCH.
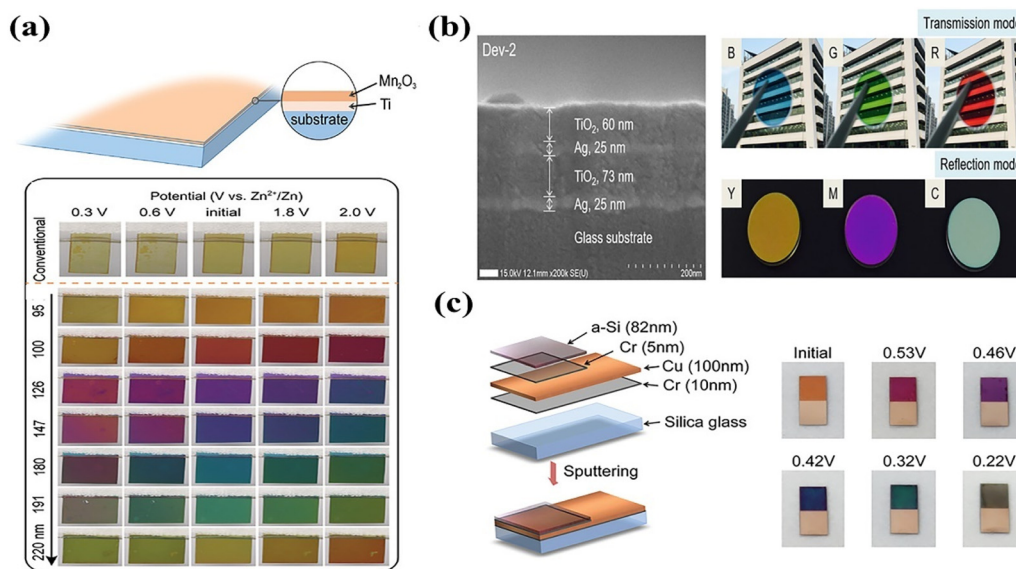

Fig. 12 (a) Structural diagram of the nano-bilayer electrochromic electrode and optical images of conventional and colorful electrochromic electrodes at different voltages. Adapted with permission from ref. 108. Copyright 2021, Wiley-VCH. (b) SEM image of the fabricated device and photographic images *via* the fabricated devices which exhibit both transmissive RGB and reflective CMY. Adapted with permission from ref. 109. Copyright 2016, Springer Nature. (c) Schematic of colorful films with an α-Si layer and photographs of the films at different voltages. Adapted with permission from ref. 110. Copyright 2018, Wiley-VCH.

the amorphous Fe_2O_3, resulting in reconfiguration of the Ag layer.[111] A considerable number of structural colors were generated in the dynamic F–P cavity structure. However, a deep understanding of the microstructure of matter is needed to achieve multicolor by ion migration, which requires a lot of research to explore its feasibility.

2.2.3 The multicolor of SPR resonance. Similar to the optical F–P cavity which generates structural color by constructive/destructive interference, plasmonic nanostructures possess the ability to encode complex color and polarization patterns due to large optical cross-sections and unique photostability. A structural color that almost covers the full color gamut can be achieved by regulating plasmonic nanostructure parameters. Correspondingly, the current strategy to generate plasmonic colors can be divided into two main strategies: (1) Structural color was generated by wavelength-selective extraordinary transmission through nanohole or nanoslit arrays, diffractive coupling in nanoparticle arrays, interference-based shaping of transmission and metal–insulator–metal devices. (2) Individual nanoparticles or plasmonic molecules are made into color-determining pixels. The former still requires a feature size of a few micrometers to generate structural color. For instance, Eric Hopmann *et al.* proposed a static plasmon metal–insulator–nanohole (MIN) cavity composed of a 100 nm gold mirror, a 120 nm WO_3 insulator, and a 20 nm gold nanopore array,[112] in which the nanohole array served both as a plasmonic light-confinement superstructure and as the transport channel for Li^+ ion de/insertion. Hence, the color experienced change continuously from red, and orange to brownish yellow corresponding to lithiation charges of 1.5 mC cm^{-2}, 3 mC cm^{-2}, and 4 mC cm^{-2} respectively. At the highest lithiation charges (6 and 8 mC cm^{-2}), the reflection became green and deep green. Highly uniform and bright colors were shown during the electrochromic process. Moreover, full color modulation was achieved after 4 s in both lithiated and delithiated cases (Fig. 13a and b). In Fig. 13c, the design of the $Al/Li_xWO_3/Al$ gap plasma structure also shows a large dynamic tuning of the resonance properties.[113]

Another strategy for structural color is the SPR effect of noble metal nanoparticles to generate plasmonic colors. SPR is the electromagnetic-field-induced collective oscillation of free electrons at the metal–dielectric interface, which enhances the light absorption and scattering of nanoparticles to achieve color modulation. The resonance wavelength of the nanoparticle is determined by the dielectric constant, size, and shape, as SPR bands of the nanoparticles can lead to dramatic changes with electrochromic redox processes. An electrochromic device based on Ag nanoparticles with transparent, silver mirror, red, blue, and black states was fabricated, making it suitable for use in information displays and light-modulating devices (Fig. 14a).[114] Further studies have revealed that the formation of metal nanoparticles involving nucleation and growth, directly determines both the size and the shape of the produced particles. The number of nucleations and the color depth of the units were usually determined by the nucleation voltage, while changes in hue were affected by growth time.[115] In addition, short nucleation times and small growth voltages typically promote the emergence of vivid colors.[116] When the nanostructure is composed of two kinds of noble metal nanoparticle, a wide range of wavelength tuning often requires the coupling of both geometric factors and material factors.[117] To date, some progress has been made in the multicolor study of the combination of electrochromic and SPR effects. For example, the application of the SPR effect of gold nanoparticles to V_2O_5 effectively broadened its primary color of yellow, green, and blue (Fig. 14b),[118] which showed good camouflage performance in common natural environments. Moving a step further, a new strategy was presented to prepare switchable films through electro-responsive dissolution and deposition of Ag on hollow shells of Au/Ag alloy.[119] When a negative bias was applied, the original lightly pigmented film became heavily pigmented, and the transparent film turned light blue, purple and finally red within 30 s, indicating the continuous growth of Au/Ag alloy nanoparticles (Fig. 14c). In addition, from −0.05 V to −0.4 V, the color of the film changed from light yellow to red and finally to blue, which was also confirmed by the decrease in the L^* value of the CIELAB chromaticity coordinates (Fig. 14d). Compared with the assembly/disassembly strategy, electrochemical switches are more suitable for practical applications because electrically driven is a more precise, dynamic, and instantaneous manner.
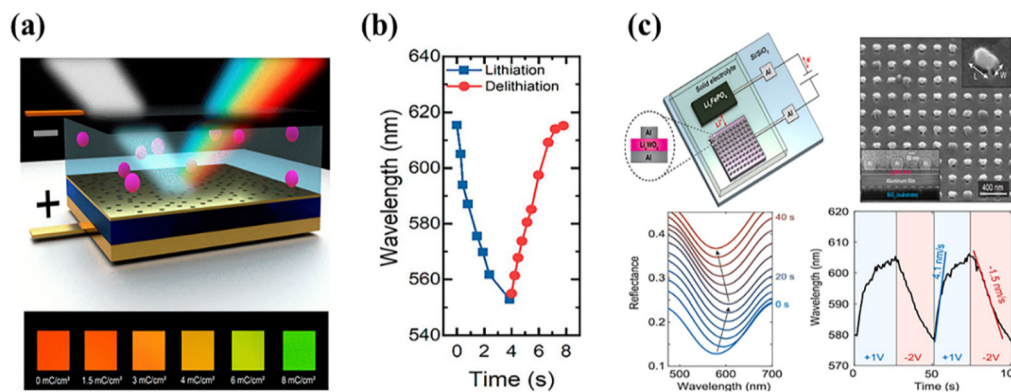

Fig. 13 (a) Schematic of a device based on an electrochromic WO_3 layer and a gold resonator. The illustration below shows images of the reflected color at various stages of the lithiation process. (b) Time dependence of the color modulation process of the device by applying −3 to 1 V potential. (a and b) Adapted with permission from ref. 112. Copyright 2020, American Chemical Society. (c) Schematic of the solid-state electrochromic device consisting of an $Al/Li_xWO_3/Al$ structure and optical responses. Adapted with permission from ref. 113. Copyright 2019, American Chemical Society.
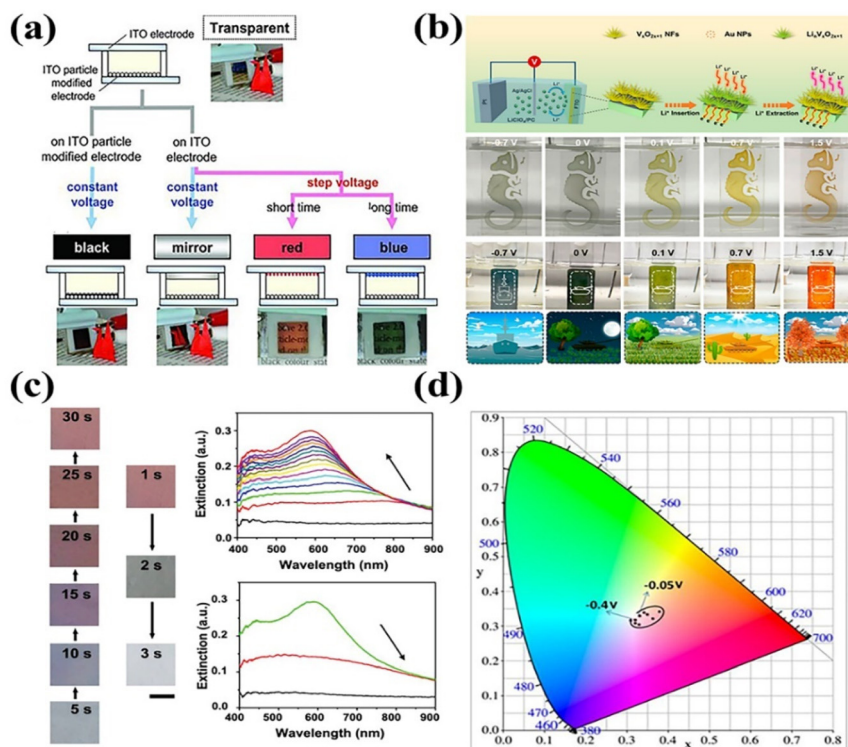
Fig. 14 A summary of using the SPR effect to achieve electrochromic multicolor. (a) Scheme and photographs of a two-electrode electrochromic cell. Adapted with permission from ref. 114. Copyright 2013, Wiley-VCH. (b) Schematic diagram of the synthesis of $Au@V_xO_{2x+1}$ nanoflowers and their application scenarios in adaptive camouflage fields. Adapted with permission from ref. 118. Copyright 2022, American Chemical Society. (c) Digital images of the Au/Ag film during the coloration and bleaching process. (d) CIE chromaticity diagram for voltage-dependent Au/Ag electrochromic films. (c and d) Adapted with permission from ref. 119. Copyright 2019, Wiley-VCH.

2.3 Multicolor constructed from an electrochromic device

Classic electrochromic devices are composed of five layers from top to bottom: namely, a transparent conductive layer, an electrochromic layer, an electrolyte layer, an ion storage layer, and a transparent conductive layer. The electrochromic layer and ion storage layer, as the most important parts of electrochromic devices, are given the ability to change color by a redox reaction at different voltages. The ion storage layer stores the ions to work with the electrochromic layer to maintain the charge balance of the entire electrochromic process. Given the above, it is possible to realize multicolor through the color superposition of different layers in the stacking structure. In order to enrich the variety of colors, Zn-sodium vanadium oxide (Zn-SVO) electrochromic displays were assembled by sandwiching Zn between two SVO electrodes (Fig. 15a).[120] Since a single SVO electrode exhibited three colors (orange, yellow, and green), six colors of the device (orange, amber, yellow, brown, chartreuse, and green) were achieved by controlling individual electrodes independently (Fig. 15b and c). In a similar three-electrode design, Wang *et al.* used WO_3 and Ti-V_2O_5 as the electrochromic active layers, and aluminum was chosen as the anode frame of the device to help seal the electrolyte.[121] For electrochromic applications, different electrode connections contribute to the multicolor capabilities of the

device (yellow, transparent, red, green, blue, and black). Notably, the flexibility of the open-circuit voltage to the energy output was facilitated by different combinations of the three-electrode design (Fig. 15d). This special design made it possible to work at multiple operating voltages, which realized the efficient use of stored energy in ECD devices. This is considered a beneficial way for devices to store green energy from solar and wind power.

More studies have demonstrated the feasibility of multicolor constructed from an electrochromic device. An all-in-organic solid-state device was assembled using Co_3O_4 and PB films as complementary electrodes with a gel electrolyte of $LiClO_4$ in the PEO matrix filled between the two electrodes,[122] and it switched between blue, green, and brown with a small bias of less than a few volts. Moreover, a moderate color contrast of about 40% with 1.5 s switching time was observed (Fig. 16a and b). Considering visual electrochromic energy storage devices, Diao *et al.* reported a multicolored EESD with PB and MnO_2 as asymmetrical electrodes to make the energy level of the device quantifiable by the chrominance difference (Fig. 16c).[123] During the charging/discharging process, various degrees of yellow, green, and blue corresponded to different energy states. To further expand the range of colors that can be displayed, the combination of WO_3 and SVO electrodes was proposed to display multiple
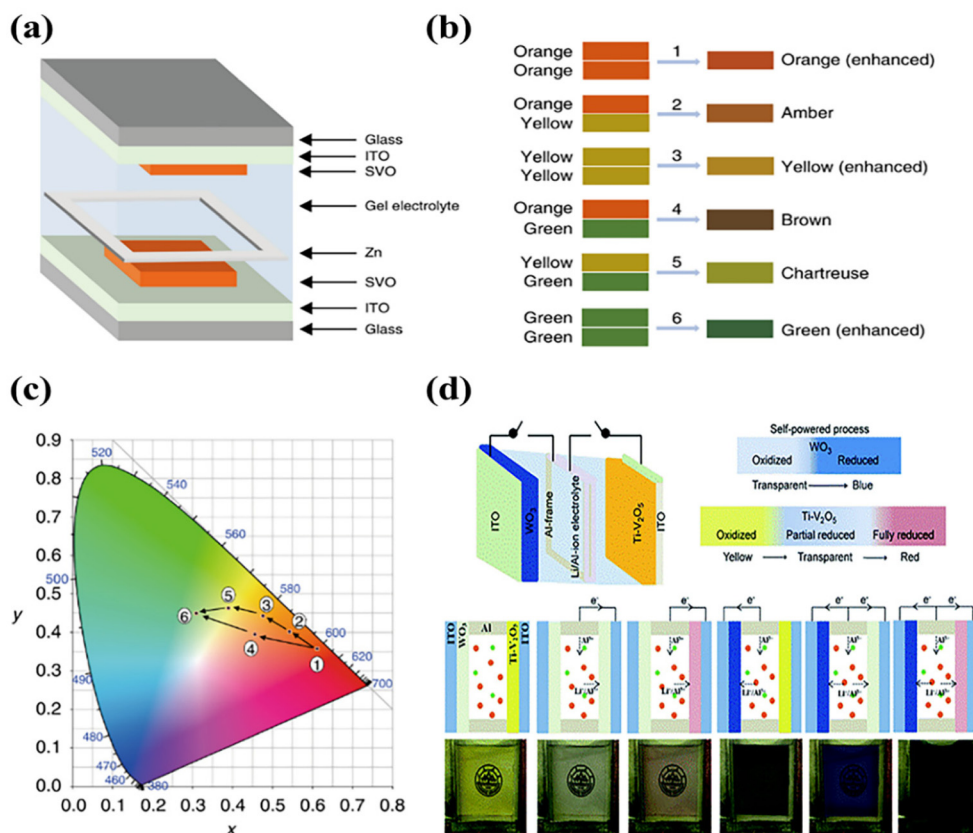
Fig. 15 (a) Design and performance of Zn-SVO electrochromic displays with broadened color palettes. (b) Schematic illustration of the color overlay effect *via* the combination of orange, yellow, and green colors. (c) CIE color coordinates of the Zn-SVO electrochromic display under different color states. (a–c) Adapted with permission from ref. 120. Copyright 2020, Springer Nature. (d) Schematic illustration of the as-assembled EESD and six different color states of the device. Adapted with permission from ref. 121. Copyright 2020, Royal Chemistry of Society.

colors traversing a 2D CIE regional color space.[124] According to previous studies of asymmetric F–P-type thin films, they had proven a good method to broaden the color hues of WO₃-based electrochromic displays. Zinc-anode-based electrochromic displays with a combination of W-WO₃ structure and SVO electrodes were fabricated to generate vivid colors, which give them further rich color tunability over a wide color gamut distribution *via* the color superposition effect (Fig. 16d–f). This unique electrochromic platform is expected to accelerate the development of multicolor for better visual effects.

Apart from the color superposition of the electrochromic layer and ion storage layer, the polychromic electrolyte should also be considered. The basic role played by the electrolytic layer in an ECD is to transport ions and block electrons. Existing studies have demonstrated that various colors can be displayed by manipulating the concentration of fluorescent labeling materials in organic solvents. Thus, designing a multicolored ECD from the perspective of an electrolyte layer is a feasible strategy. As a typical fluorescent labeling material, doping with carbon dots (CDs) can effectively improve the conductivity of electrolytes. The increase in conductivity can also indirectly enhance the performance of elec-

trochromic devices. An ECD was successfully fabricated by employing MnO₂ and PB as complementary electrodes and meanwhile introducing CDs into the electrolyte layers.[125] The device initially appeared orange-red at 0 V, but with increasing voltage, its color transitioned gradually from orange-red to orange, light yellow, yellow, green, and finally to dark green (Fig. 17a). Similarly, incorporating diverse pigments consisting of oxides and small molecules into the electrolyte solution can attain the desired color of the electrolyte layer. Rougier *et al.* used WO₃ as the working electrode, and V₂O₅ with embedded lithium as the counter-electrode. TiO₂ was added to Jaune 920, Rouge 110, Vert 4FR, and colorless gel electrolytes to obtain the corresponding yellow, red, green, and white (Fig. 17b).[126] An ECD composed of gel electrolyte layers with four different pigments showed great color contrast between their reduced state and oxidation state. This is different from the coloration mechanism of most electrochromic devices, where the color change of the pH indicator caused by external stimuli represents an emerging electrochromic mechanism. Huang *et al.* adjusted the basicity of the electrolyte to make Co₃O₄ nanosheets colored by the color change of the pH indicator.[127] Based on the color changes of phenolphthalein (PP), thymolphthalein (TP), and
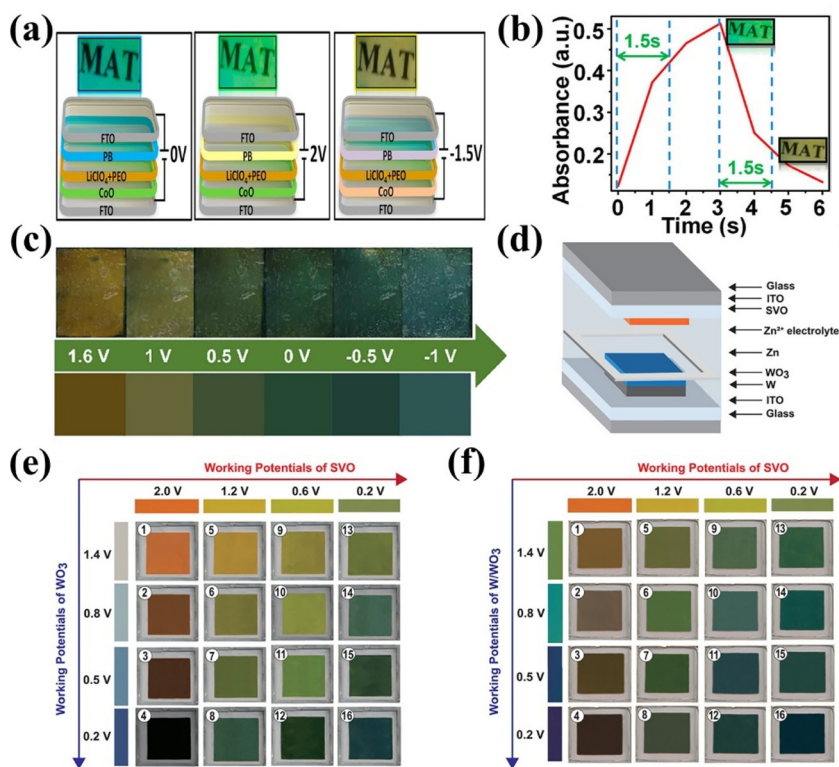
Fig. 16 (a) Schematic illustration of fabricated device under different voltages (0 V, 2 V, −1 V). (b) One absorbance switching cycle of the device under bias pulse with extreme biases of 2 V and −1.5 V. (a and b) Adapted with permission from ref. 122. Copyright 2020, American Chemical Society. (c) Real photographs (up) and emulation images (down) in charging and discharging processes. Adapted with permission from ref. 123. Copyright 2023, American Chemical Society. (d) Schematic illustration of the fabricated SVO-Zn-WO$_3$ electrochromic display. (e and f) Digital images of the SVO-Zn-WO$_3$ display and SVO-Zn-WO$_3$/W display. (d–f) Adapted with permission from ref. 124. Copyright 2021, Wiley-VCH.
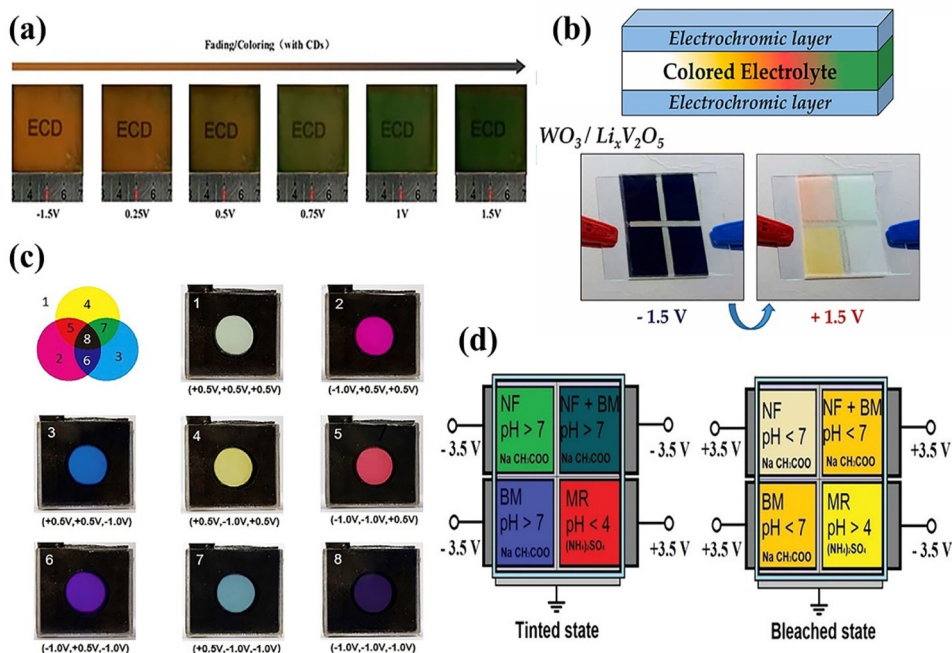

Fig. 17 (a) Color of ECDs at different potentials with CDS. Adapted with permission from ref. 125. Copyright 2022, Frontiers Media S.A. (b) Photographs of the multicolored WO$_3$/electrolyte/Li$_x$V$_2$O$_5$ display with four colored electrolytes. Adapted with permission from ref. 126 Copyright 2022, Elsevier. (c) Color palette of electrochromic windows. Adapted with permission from ref. 127. Copyright 2019, Elsevier. (d) Schematic representation of the assembled four-pixel device in different states. Adapted with permission from ref. 128. Copyright 2022, Wiley-VCH.

Table 3 Summary of recent progress in multicolor based on inorganic electrochromic materials

Category	EC material	Feature	Color	Cycle stability	Ref.
Vanadium oxides	V_2O_5	Nanobelt (6 cm × 6 cm)	Gray–yellow–brick red	94% (after 1000 cycles)	73
		Nanosheet	Yellow–green–blue	79.7% (after 200 cycles)	77
		Coralline	Aquamarine–orange–olive	—	78
		SnO_2/V_2O_5 core/shell	Yellow–green–blue	85% (after 2000 cycles)	79
		V_2O_5@C Microrod (10 cm × 10 cm)	Yellow–gray-green–bice	96% (after 2000 cycles)	74
	V_3O_7	Colloidal nanoparticle	Bice–yellow	—	81
	V_2O_3	High crystallinity	Green–blue–orange		80
Prussian blue analogs	PG	—	Green–blue–colorless	—	84
	$K_2Co[Fe(CN)_6]$	—	Light green–reddish brown	—	88
	$K_2Cu[Fe(CN)_6]$	—	Light yellow–red	—	89
	MoOHCF	—	Brown-red–light yellow	>95% (after 300 cycles)	85
Other composite films	WO_3-V_2O_5	V_2O_5 dots-WO_3 nanorod	Black–green yellow–orange-yellow	—	90
		WO_3/V_2O_5 nanowires	Light orange–blue-gray	—	91
	CdS/WO_3	CdS QDs	Yellow–black–green–brown	>90% (after 1000 cycles)	93
	$Co(OH)_2/Ni(OH)_2$	Core/shell	Yellow–green–brown	—	94
	FeHCF-MoOHCF	—	Red–green–blue–yellow	>1000 cycles	95
Photon metamaterial	WO_3	ECDBR	Wide color gamut	—	35
	NiO	Inverse opal	Blue–red	>500 cycles	96
	PB	SiO_2@PB core/shell	White–blue–green	>200 cycles	97
	WO_3 NiO	1D photonic crystal	Green–pink–yellow	—	98
F–P cavity	WO_3	Ag-WO_3-Ag	Full colors	—	101
		W-WO_3	Full colors	81% (after 1000 cycles)	102
		WO_3-ITO-Ag-ITO-Ag	Wide color gamut	—	104
		Cr-WO_3-Al	Full colors	>500 cycles	105
		Au-WO_3-Pt	Full colors	—	106
		WO_3-W-nylon-66 (5 cm × 5 cm)	Large color gamut	—	107
	Mn_2O_3	Ti-Mn_2O_3 (3 cm × 3 cm)	Wide color gamut	—	108
	TiO_2	Ag-TiO_2-Ag-TiO_2	Wide color gamut	—	109
	Si	Si-Cr-Cu-Cr	Full colors	—	110
	Fe_2O_3	Ag-Fe_2O_3	Full colors	—	111
SPR	WO_3	Ag-WO_3-Ag (2.8 cm × 1.5 cm)	Full colors	—	112
	Li_xWO_3	Al-Li_xWO_3	Wide color gamut	—	113
	Ag	nanoparticle	Red–blue–black	—	114
	V_2O_5	Au-V_2O_5 nanoflower	Orange–yellow–green–gray-blue	>2000 cycles	118
Device	Au/Ag	Core/shell (1 cm × 4 cm)	Wide color gamut	—	119
	SVO	SVO-Zn-SVO (2 cm × 5 cm)	Wide color gamut	—	120
	W-WO_3 SVO	W-WO_3 F P cavity	Sixteen colors	—	124
	WO_3-Ti-V_2O_5	WO_3-Al-Ti-V_2O_5 (5 cm × 5 cm)	Six colors	—	121
	WO_3 V_2O_5	Jaune 920, Rouge 110, Vert 4FR, TiO_2 electrolyte	Yellow–red–green–white	—	126
	PH indicator	PP, TP, 3-nitrophenol (32 cm × 18 cm)	Eight colors	—	127
		NF, BM, MR	Wide color gamut	—	128
	PB MnO_2	PB/$LiClO_4$ + CDS/MnO_2	Orange–yellow–green	>1000 cycles	125
		All-solid-state	Multicolor	>500 cycles	123
	PB Co_3O_4	—	Blue–green–brown	>300 cycles	122

3-nitrophenol (yellow) in the electrolyte, various colors, including colorless, red, blue, yellow, red-orange, purple, green, and dark blue, were observed. Compared with a conventional electrochromic device, this novel electrochromic device had a wider color gamut and larger fabrication areas (32 cm × 18 cm), which demonstrated the potential of pH chemical tuning in electrolytes for future electrochromic window applications (Fig. 17c). In order to improve the applicability of such electrochromic devices, Rozman *et al.* developed a novel method by combining a PH indicator dye and aqueous electrolyte with a readily available stainless-steel sheet, which regulated the color changes of α-naphtholphthalein (NF), methyl red (MR) and bromothymol blue (BM) in Fig. 17d.[128] The low-cost multicolor device eliminated the potential fire hazards of organic and polymer electrodes, while the water-soluble electrolyte greatly improves its maintainability, making it more suitable for use in less developed or remote areas.

3. Summary and prospects

Dazzling and colorful designs and multifunctional electronic products are prompting researchers to develop advanced electrochromic materials to meet the desires for multicolor. This review has provided a detailed overview of recent advances in multicolor based on inorganic electrochromic materials in Table 3. Three main strategies have been proposed to realize multicolor using inorganic electrochromic technology. Accordingly, a set of interesting applications were derived from the multicolor of intrinsic colors and electrochromic devices. For instance, electrochromic intelligent windows were fabricated, which can adjust the intensity of incident light and transform colors to realize artistic beauty. In the military, multicolored electrochromic coating materials that change with different environments will greatly improve the ability of self-adaptive camouflage. However, the hue, chroma, and purity of colors are greatly affected by the internal microstructure of the material itself. Colors with limited variety and low purity have been shown to be improved by the more reasonable design of nanostructures and new combinations of electrochromic materials.

In fact, significant color changes come mainly from the reflectance mediated by the interaction of different layers, rather than from the material itself in most cases. The predesigned optical structures and SPR effect of nanoparticles are used to enhance the interference of light to develop a multicolored ECD. The type of multicolor based on structural colors greatly expands the color gamut, improving the brightness and purity of light. But there is still a lot of work to be done to introduce electrochromic multicolor to daily life. There are still some outstanding challenges that need to be overcome in future research:

(1) To achieve large-scale commercialization of inorganic electrochromic multicolor devices, it is necessary to rule out expensive and complex electron or ion beam lithography. The use of simpler and cheaper chemical/physical vapor deposition processes, nanoimprint, and colloidal lithography requires further demonstration, all of which have some advantages of cost-effectiveness and repeatability and will lay a good foundation for large-scale applications.

(2) At present, optical resonators represented by photonic crystals and F–P cavities have proven to be an important method for the multicolored tuning of inorganic electrochromic materials. An exploration of new combinations between inorganic electrochromic materials and more suitable optical resonators such as the Mie resonator is expected to obtain structural colors with higher quality. In addition, by a combination of multiple resonators, the shortcomings of a single resonator will be improved, which include tunable color chrominance, a narrow viewing angle, and a long response time.

(3) In nature, there are other ways to produce colors, such as the coloring reaction of iodine and starch and the tunable structural colors produced by liquid crystals. The combination of new methods with electrochromic materials is expected to expand the range of color gamut.

With the discovery of new materials and the continuous integration and upgrading of various advanced manufacturing processes, inorganic electrochromic multicolored materials with better performance and lower cost will prompt more interesting products in the future. The active exploration of this interesting scientific field requires the joint efforts of a broad number of scientific researchers and outstanding engineers.

Conflicts of interest

The authors declare no conflict of interest.

Acknowledgements

References

1 Y. Ma, S. J. Xin, X. Liu, Y. Liu, J. Sun, X. Wang, Q. Guo and V. G. Chigrinov, *Liq. Cryst.*, 2020, **47**, 1729–1734.

2 G. Cai, J. Wang and P. S. Lee, *Acc. Chem. Res.*, 2016, **49**, 1469–1476.

3 Y. Kim, C. Park, S. Im and J. H. Kim, *Sci. Rep.*, 2020, **10**, 16488.

4 W. Wu, M. Wang, J. Ma, Y. Cao and Y. Deng, *Adv. Electron. Mater.*, 2018, **4**, 1800185.

5 L. Shao, X. Zhuo and J. Wang, *Adv. Mater.*, 2018, **30**, 1704338.

6 S. Sinha, R. Daniels, O. Yassin, M. Baczkowski, M. Tefferi, A. Deshmukh, Y. Cao and G. Sotzing, *Adv. Mater. Technol.*, 2021, **7**, 2100548.

7 Z. Li, Y. Zhao, Y. Xiao, W. Sun, M. Chen, W. Li, X. Zhang, J. Zhao and Y. Li, *Mater. Lett.*, 2022, **307**, 130969.

8 P. Zhao, H. Chen, B. Li, H. Tian, D. Lai and Y. Gao, *Opt. Mater.*, 2019, **94**, 378–386.

9 D. S. Dalavi, R. S. Desai and P. S. Patil, *J. Mater. Chem. A*, 2022, **10**, 1179–1226.

10 Z. Luo, L. Liu, X. Yang, X. Luo, P. Bi, Z. Fu, A. Pang, W. Li and Y. Yi, *ACS Appl. Mater. Interfaces*, 2020, **12**, 39098–39107.

11 M. Tian, X. Liu, X. Diao and X. Zhong, *Sol. Energy Mater. Sol. Cells*, 2023, **253**, 112239.

12 Y. Zhong, Z. Chai, Z. Liang, P. Sun, W. Xie, C. Zhao and W. Mai, *ACS Appl. Mater. Interfaces*, 2017, **9**, 34085–34092.

13 Y. Wang, S. Wang, X. Wang, W. Zhang, W. Zheng, Y. M. Zhang and S. X. Zhang, *Nat. Mater.*, 2019, **18**, 1335–1342.

14 R. J. Mortimer, *Annu. Rev. Mater. Res.*, 2011, **41**, 241–268.

15 Y. Jiang, Z. Xian, Y. Meng, G. Zhou, C. Cabanetos, J. Roncali, J.-m. Liu and J. Gao, *Dyes Pigm.*, 2019, **162**, 697–703.

16 M. Kim, Y. M. Kim and H. C. Moon, *RSC Adv.*, 2019, **10**, 394–401.

17 B. B. Carbas, *Polymer*, 2022, **254**, 125040.

18 F. Hu, B. Yan, G. Sun, J. Xu, Y. Gu, S. Lin, S. Zhang, B. Liu and S. Chen, *ACS Appl. Nano Mater.*, 2019, **2**, 3154–3160.

19 L. Huang, S. Cao, Y. Liang, J. Chen, T. Yang, J. Zhao and B. Zou, *J. Mater. Chem. C*, 2023, **11**, 10107–10120.

20 K. J. Patel, G. G. Bhatt, J. R. Ray, P. Suryavanshi and C. J. Panchal, *J. Solid State Electrochem.*, 2016, **21**, 337–347.

21 N. Y. Bhosale, S. S. Mali, C. K. Hong and A. V. Kadam, *Electrochim. Acta*, 2017, **246**, 1112–1120.

22 S. K. Deb, *Appl. Opt.*, 1969, **8**, 192–195.

23 A. Khan, B. Nilam, C. Rukhsar, G. Sayali, B. Mandlekar and A. Kadam, *Tungsten*, 2022, 87.

24 P. Yang, P. Sun and W. Mai, *Mater. Today*, 2016, **19**, 394–402.

25 Y. Li, J. Zhao, X. Chen, L. Wang, W. Li and X. Zhang, *J. Inorg. Mater.*, 2021, **36**, 451.

26 W. He, Y. Liu, Z. Wan and C. Jia, *RSC Adv.*, 2016, **6**, 68997–69006.

27 H. Liu, X. Liang, T. Jiang, Y. Zhang, S. Liu, X. Wang, X. Fan, X. Huai, Y. Fu, Z. Geng and D. Zhang, *Sol. Energy Mater. Sol. Cells*, 2022, **238**, 111627.

28 J. Y. Zheng, Q. Sun, J. Cui, X. Yu, S. Li, L. Zhang, S. Jiang, W. Ma and R. Ma, *Nanoscale*, 2022, **15**, 63–79.

29 J. Eaves-Rathert, E. Kovalik, C. F. Ugwu, B. R. Rogers, C. L. Pint and J. G. Valentine, *Nano Lett.*, 2022, **22**, 1626–1632.

30 K. Xiong, O. Olsson, J. Svirelis, C. Palasingh, J. Baumberg and A. Dahlin, *Adv. Mater.*, 2021, **33**, 2103217.

31 L. Liu, Q. Zhang, K. Du, Z. He, T. Wang, Y. Yi, M. Wang, X. Zhong, G. Dong and X. Diao, *J. Mater. Chem. A*, 2019, **7**, 23028–23037.

32 S. Oukassi, C. Giroud-Garampon, C. Dubarry, C. Ducros and R. Salot, *Sol. Energy Mater. Sol. Cells*, 2016, **145**, 2–7.

33 A. Jarry, M. Walker, S. Theodoru, L. J. Brillson and G. W. Rubloff, *Chem. Mater.*, 2020, **32**, 7226–7236.

34 R. J. Mortimer and T. S. Varley, *Sol. Energy Mater. Sol. Cells*, 2013, **109**, 275–279.

35 L. Xiao, Y. Lv, J. Lin, Y. Hu, W. Dong, X. Guo, Y. Fan, N. Zhang, J. Zhao, Y. Wang and X. Liu, *Adv. Opt. Mater.*, 2018, **6**, 1700791.

36 J. S. King, E. Graugnard and C. J. Summers, *Adv. Mater.*, 2005, **17**, 1010–1013.

37 H. Li, Z. Tang, Y. Liu, J. Robichaud, J. Liang, W. Jiang and Y. Djaoued, *Materials*, 2022, **15**, 2904.

38 Y. Zhan, Z. Yang, Z. Xu, Z. Hu, X. Bai, Y. Ren, M. Li, A. Ullah, I. Khan, J. Qiu, Z. Song, B. Liu and Y. Wang, *Chem. Eng. J.*, 2020, **394**, 124967.

39 K. Chen, Q. Fu, S. Ye and J. Ge, *Adv. Funct. Mater.*, 2017, **27**, 1702825.

40 W. Li, Y. Wang, M. Li, L. P. Garbarini and F. G. Omenetto, *Adv. Mater.*, 2019, **31**, 1901036.

41 S. Rossi, O. Olsson, S. Chen, R. Shanker, D. Banerjee, A. Dahlin and M. P. Jonsson, *Adv. Mater.*, 2021, **33**, e2105004.

42 X. Wang, K. Chen, L. S. de Vasconcelos, J. He, Y. C. Shin, J. Mei and K. Zhao, *Nat. Commun.*, 2020, **11**, 211.

43 J. Zhao, M. Qiu, X. Yu, X. Yang, W. Jin, D. Lei and Y. Yu, *Adv. Opt. Mater.*, 2019, **7**, 1900646.

44 D. D. Evanoff Jr. and G. Chumanov, *ChemPhysChem*, 2005, **6**, 1221–1231.

45 T. R. Gordon, T. Paik, D. R. Klein, G. V. Naik, H. Caglayan, A. Boltasseva and C. B. Murray, *Nano Lett.*, 2013, **13**, 2857–2863.

46 Z. Liang, K. Nakamura and N. Kobayashi, *Sol. Energy Mater. Sol. Cells*, 2019, **200**, 109914.

47 W. Zhang, H. Li, E. Hopmann and A. Y. Elezzabi, *Nanophotonics*, 2020, **10**, 825–850.

48 M. A. Arvizu, H. Y. Qu, U. Cindemir, Z. Qiu, E. A. Rojas-Gonzalez, D. Primetzhofer, C. G. Granqvist, L. Osterlund and G. A. Niklasson, *J. Mater. Chem. A*, 2019, **7**, 2908–2918.

49 W. Yang, X. Du, J. Zhao, Z. Chen, J. Li, J. Xie, Y. Zhang, Z. Cui, Q. Kong, Z. Zhao, C. Wang, Q. Zhang and G. Cui, *Joule*, 2020, **4**, 1557–1574.

50 A. Sood, A. D. Poletayev, D. A. Cogswell, P. M. Csernica, J. T. Mefford, D. Fraggedakis, M. F. Toney, A. M. Lindenberg, M. Z. Bazant and W. C. Chueh, *Nat. Rev. Mater.*, 2021, **6**, 847–867.

51 A. C. Sonavane, A. I. Inamdar, P. S. Shinde, H. P. Deshmukh, R. S. Patil and P. S. Patil, *J. Alloys Compd.*, 2010, **489**, 667–673.

52 B. W. Faughnan, R. S. Crandall and M. A. Lampert, *Appl. Phys. Lett.*, 1975, **27**, 275–277.

53 X. Zhang, Y. Tian, W. Li, S. Dou, L. Wang, H. Qu, J. Zhao and Y. Li, *Sol. Energy Mater. Sol. Cells*, 2019, **200**, 109916.

54 P. R. Bueno, C. Gabrielli and H. Perrot, *Electrochim. Acta*, 2008, **53**, 5533–5539.

55 Ö. D. Coşkun, S. Demirel and G. Atak, *J. Alloys Compd.*, 2015, **648**, 994–1004.

56 R. T. Wen, G. A. Niklasson and C. G. Granqvist, *ACS Appl. Mater. Interfaces*, 2016, **8**, 5777–5782.

57 S. Zhang, S. Cao, T. Zhang and J. Y. Lee, *Adv. Mater.*, 2020, **32**, e2004686.

58 A. Arash, S. A. Tawfik, M. J. S. Spencer, S. K. Jain, S. Arash, A. Mazumder, E. Mayes, F. Rahman, M. Singh, V. Bansal, S. Sriram, S. Walia, M. Bhaskaran and S. Balendhran, *ACS Appl. Mater. Interfaces*, 2020, **12**, 16997–17003.

59 W. Zhang, H. Li, C. J. Firby, M. Al-Hussein and A. Y. Elezzabi, *ACS Appl. Mater. Interfaces*, 2019, **11**, 20378–20385.

60 X. Che, Z. Wu, G. Dong, X. Diao, Y. Zhou, J. Guo, D. Dong and M. Wang, *Thin Solid Films*, 2018, **662**, 6–12.

61 S. Bogati, R. Basnet and A. Georg, *Sol. Energy Mater. Sol. Cells*, 2019, **189**, 206–213.

62 C. R. Dhas, R. Venkatesh, R. Sivakumar, A. M. E. Raj and C. Sanjeeviraja, *Opt. Mater.*, 2017, **72**, 717–729.

63 D. Ma, A. Lee-Sie Eh, S. Cao, P. S. Lee and J. Wang, *ACS Appl. Mater. Interfaces*, 2022, **14**, 1443–1451.

64 Y. S. Nam, H. Park, A. P. Magyar, D. S. Yun, T. S. Pollom Jr. and A. M. Belcher, *Nanoscale*, 2012, **4**, 3405–3409.

65 Y. Ren, X. Zhou, H. Zhang, L. Lei and G. Zhao, *J. Mater. Chem. C*, 2018, **6**, 4952–4958.

66 S. Sajitha, U. Aparna and B. Deb, *Adv. Mater. Interfaces*, 2019, **6**, 1901038.

67 H. Yang, J.-H. Yu, H. J. Seo, R. H. Jeong and J.-H. Boo, *Appl. Surf. Sci.*, 2018, **461**, 88–92.

68 H. Zhao, Y. Meng, H. Yu, Z. Li and Z. Liu, *Ceram. Int.*, 2022, **48**, 32205–32212.

69 C. G. Granqvist, *Appl. Phys. A: Mater. Sci. Process.*, 1993, **57**, 3–12.

70 E. L. Runnerstrom, A. Llordes, S. D. Lounis and D. J. Milliron, *Chem. Commun.*, 2014, **50**, 10555–10572.

71 Y. Liu, C. Jia, Z. Wan, X. Weng, J. Xie and L. Deng, *Sol. Energy Mater. Sol. Cells*, 2015, **132**, 467–475.

72 I. Mjejri, L. M. Manceriu, M. Gaudon, A. Rougier and F. Sediri, *Solid State Ionics*, 2016, **292**, 8–14.

73 S. Zhang, S. Chen, Y. Luo, B. Yan, Y. Gu, F. Yang and Y. Cao, *J. Alloys Compd.*, 2020, **842**, 155882.

74 H. Li, H. Liang, R. Li, Z. Lu, C. Hou, Q. Zhang, Y. Li, K. Li and H. Wang, *ACS Appl. Mater. Interfaces*, 2022, **14**, 48037–48044.

75 D. Cho, H. Chen, J. Shin and S. Jeon, *Nanophotonics*, 2022, **11**, 2737–2762.

76 D. Ge, E. Lee, L. Yang, Y. Cho, M. Li, D. S. Gianola and S. Yang, *Adv. Mater.*, 2015, **27**, 2489–2495.

77 J. Kim, K. H. Lee, S. Lee, S. Park, H. Chen, S. K. Kim, S. Yim, W. Song, S. S. Lee, D. H. Yoon, S. Jeon and K.-S. An, *Chem. Eng. J.*, 2023, **453**, 139973.

78 Z. Tong, N. Li, H. Lv, Y. Tian, H. Qu, X. Zhang, J. Zhao and Y. Li, *Sol. Energy Mater. Sol. Cells*, 2016, **146**, 135–143.

79 G.-f. Zhao, W.-q. Wang, X.-l. Wang, X.-h. Xia, C.-d. Gu and J.-p. Tu, *J. Mater. Chem. C*, 2019, **7**, 5702–5709.

80 I. Mjejri, M. Gaudon, G. Song, C. Labrugère and A. Rougier, *ACS Appl. Energy Mater.*, 2018, **1**, 2721–2729.

81 W. Zhang, H. Li, M. Al–Hussein and A. Y. Elezzabi, *Adv. Opt. Mater.*, 2019, **8**, 1901224.

82 J. Qian, D. Ma, Z. Xu, D. Li and J. Wang, *Sol. Energy Mater. Sol. Cells*, 2018, **177**, 9–14.

83 J. Chu, X. Li, Y. Cheng and S. Xiong, *Mater. Lett.*, 2020, **258**, 126782.

84 F. Li, D. Ma, J. Qian, B. Yang, Z. Xu, D. Li, Z. Wu and J. Wang, *Sol. Energy Mater. Sol. Cells*, 2019, **192**, 103–108.

85 H.-Y. Liao, T.-C. Liao, W.-H. Chen, C.-H. Chang and L.-C. Chen, *Sol. Energy Mater. Sol. Cells*, 2016, **145**, 8–15.

86 S.-F. Hong and L.-C. Chen, *Sol. Energy Mater. Sol. Cells*, 2012, **104**, 64–74.

87 T.-C. Liao, W.-H. Chen, H.-Y. Liao and L.-C. Chen, *Sol. Energy Mater. Sol. Cells*, 2016, **145**, 26–34.

88 S. Pahal, M. Deepa, S. Bhandari, K. N. Sood and A. K. Srivastava, *Sol. Energy Mater. Sol. Cells*, 2010, **94**, 1064–1075.

89 M. K. Sharma and S. K. Aggarwal, *J. Electroanal. Chem.*, 2013, **705**, 64–67.

90 K. Tang, Y. Zhang, Y. Shi, J. Cui, X. Shu, Y. Wang, J. Liu, J. Wang, H. H. Tan and Y. Wu, *J. Mater. Chem. C*, 2018, **6**, 12206–12216.

91 J. L. Wang, J. W. Liu, S. Z. Sheng, Z. He, J. Gao and S. H. Yu, *Nano Lett.*, 2021, **21**, 9203–9209.

92 C. J. Wang, M. Shim and P. Guyot-Sionnest, *Science*, 2001, **291**, 2390–2392.

93 B. Zhang, H. Wang, Y. Xiang, H. Jiang, L. Tang, J. Luo and Y. Tian, *Electrochim. Acta*, 2023, **440**, 141749.

94 Y.-H. Lee, J. S. Kang, J.-H. Park, J. Kang, I.-R. Jo, Y.-E. Sung and K.-S. Ahn, *Nano Energy*, 2020, **72**, 104720.

95 X. Zou, Y. Wang, Y. Tan, J. Pan, J. Niu and C. Jia, *ACS Appl. Mater. Interfaces*, 2020, **12**, 29432–29442.

96 H.-Y. Qu, J. Wang, J. Montero, Y. Li, L. Österlund and G. A. Niklasson, *J. Appl. Phys.*, 2021, **129**, 123105.

97 Q. Zhang, X. Li, M. Qin, F. Guan, Y. Gong, R. Wang, J. Xu and G. Chen, *ACS Appl. Electron. Mater.*, 2021, **3**, 4441–4447.

98 E. Redel, J. Mlynarski, J. Moir, A. Jelle, C. Huai, S. Petrov, M. G. Helander, F. C. Peiris, G. von Freymann and G. A. Ozin, *Adv. Mater.*, 2012, **24**, 265–269.

99 Y. Bu, X. Bu, F. Lyu, G. Liu, G. Wu, L. Pan, L. Cheng, J. C. Ho and J. Lu, *Adv. Opt. Mater.*, 2019, **8**, 1901626.

100 Z. Yang, Y. Zhou, Y. Chen, Y. Wang, P. Dai, Z. Zhang and H. Duan, *Adv. Opt. Mater.*, 2016, **4**, 1196–1202.

101 Y. Lee, J. Yun, M. Seo, S. J. Kim, J. Oh, C. M. Kang, H. J. Sun, T. D. Chung and B. Lee, *Nano Lett.*, 2020, **20**, 6084–6090.

102 Z. Wang, X. Wang, S. Cong, J. Chen, H. Sun, Z. Chen, G. Song, F. Geng, Q. Chen and Z. Zhao, *Nat. Commun.*, 2020, **11**, 302.

103 J. Chen, Z. Wang, Z. Chen, S. Cong and Z. Zhao, *Nano Lett.*, 2020, **20**, 1915–1922.

104 J. Chen, Y. Li, T. Zhang, X. Zha, X. Tang, X. Mu, P. Sun, G. Song, S. Cong, Q. Chen and Z. Zhao, *Laser Photonics Rev.*, 2022, **16**, 2200303.

105 L. Zheng, S. Zhang, Q. Yao, K. Lin, A. Rao, C. Niu, M. Yang, L. Wang and Y. Lv, *Ceram. Int.*, 2023, **49**, 13355–13362.

106 M. Gugole, O. Olsson, S. Rossi, M. P. Jonsson and A. Dahlin, *Nano Lett.*, 2021, **21**, 4343–4350.

107 Y. Li, P. Sun, J. Chen, X. Zha, X. Tang, Z. Chen, Y. Zhang, S. Cong, F. Geng and Z. Zhao, *Adv. Mater.*, 2023, **35**, 2300116.

108 X. Tang, J. Chen, Z. Wang, Z. Hu, G. Song, S. Zhang, Z. Chen, Q. Wu, M. Liu, S. Cong and Z. Zhao, *Adv. Opt. Mater.*, 2021, **9**, 2100637.

109 C. S. Park, V. R. Shrestha, S. S. Lee and D. Y. Choi, *Sci. Rep.*, 2016, **6**, 25496.

110 Y. Bao, Y. Han, L. Yang, N. Li, J. Luo, W. Qu, R. Chen, A. K. Y. Jen, T. Li, H. Chen, W.-L. Song and D. Fang, *Adv. Funct. Mater.*, 2019, **29**, 1806383.

111 Z. Yan, Z. Zhang, W. Wu, X. Ji, S. Sun, Y. Jiang, C. C. Tan, L. Yang, C. T. Chong, C. W. Qiu and R. Zhao, *Nat. Nanotechnol.*, 2021, **16**, 795–801.

112 E. Hopmann and A. Y. Elezzabi, *Nano Lett.*, 2020, **20**, 1876–1882.

113 Y. Li, J. van de Groep, A. A. Talin and M. L. Brongersma, *Nano Lett.*, 2019, **19**, 7988–7995.

114 A. Tsuboi, K. Nakamura and N. Kobayashi, *Adv. Mater.*, 2013, **25**, 3197–3201.

115 Z. He, X. Yuan, Q. Wang, L. Yu, C. Zou, C. Li, Y. Zhao, B. He, L. Zhang, H. Zhang and H. Yang, *Adv. Opt. Mater.*, 2015, **4**, 106–111.

116 A. Tsuboi, K. Nakamura and N. Kobayashi, *Sol. Energy Mater. Sol. Cells*, 2016, **145**, 16–25.

117 G. Wang, X. Chen, S. Liu, C. Wong and S. Chu, *ACS Nano*, 2016, **10**, 1788–1794.

118 B. Wang, Y. Huang, Y. Han, W. Zhang, C. Zhou, Q. Jiang, F. Chen, X. Wu, R. Li, P. Lyu, S. Zhao, F. Wang and R. Zhang, *Nano Lett.*, 2022, **22**, 3713–3720.

119 N. Li, P. Wei, L. Yu, J. Ji, J. Zhao, C. Gao, Y. Li and Y. Yin, *Small*, 2019, **15**, e1804974.

120 W. Zhang, H. Li, W. W. Yu and A. Y. Elezzabi, *Light: Sci. Appl.*, 2020, **9**, 121.

121 L. Wang, M. Guo, J. Zhan, X. Jiao, D. Chen and T. Wang, *J. Mater. Chem. A*, 2020, **8**, 17098–17105.

122 A. Chaudhary, D. K. Pathak, T. Ghosh, S. Kandpal, M. Tanwar, C. Rani and R. Kumar, *ACS Appl. Electron. Mater.*, 2020, **2**, 1768–1773.

123 Y. Ding, M. Wang, Z. Mei and X. Diao, *ACS Appl. Mater. Interfaces*, 2023, **15**, 15646–15656.

124 W. Zhang, H. Li and A. Y. Elezzabi, *Adv. Funct. Mater.*, 2021, **32**, 2108341.

125 C. Li, M. Zhen, B. Sun, Y. Hong, J. Xiong, W. Xue, X. Li, Z. Guo and L. Liu, *Front. Chem.*, 2022, **10**, 1001531.

126 C. Périé, V. Mary, B. Faceira and A. Rougier, *Sol. Energy Mater. Sol. Cells*, 2022, **238**, 111626.

127 Y. Huang, C. Yang, B. Deng, C. Wang, Q. Li, C. De Villenoisy Thibault, K. Huang, K. Huo and H. Wu, *Nano Energy*, 2019, **66**, 104200.

128 M. Rozman, *Adv. Electron. Mater.*, 2021, **8**, 2100901.